DESIGN & PERFORMANCE OF A WIND AND SOLAR-POWERED AUTONOMOUS SURFACE VEHICLE

by

Patrick Forde Rynne

A Thesis Submitted to the Faculty of

The College of Computer Science and Engineering

in Partial Fulfillment of the Requirements for the Degree of

Master of Science

Florida Atlantic University

Boca Raton, Florida

December 2008

DESIGN & PERFORMANCE OF A WIND AND SOLAR-POWERED AUTONOMOUS SURFACE VEHICLE

by

Patrick Rynne

This thesis was prepared under the direction of the candidate's thesis advisor, Dr. Karl von Ellenrieder, Department of Ocean Engineering, and has been approved by the members of his supervisory committee. It was submitted to the faculty of the College of Engineering and Computer Science and was accepted in partial fulfillment of the requirements for the degree of Master of Science.

SUPERVISORY COMMITTEE:

Karl von Ellenrieder, Ph.D.
Thesis Advisor

George Frisk, Ph.D.

David Palmer, Ph.D.

Manhar Dhanak, Ph.D.
Chair, Department of Ocean Engineering

Karl K. Stevens, Ph.D., P.E.
Dean, College of Engineering and Computer Science

Barry T. Rosson, Ph.D.
Dean, Graduate College

Nov. 24, 2008
Date

ABSTRACT

Author:	Patrick Forde Rynne
Title:	Design & Performance of a Wind and Solar-Powered Autonomous Surface Vehicle
Thesis Advisor:	Dr. Karl von Ellenrieder
Degree:	Master of Science
Year:	2008

The primary objective of this research is the development a wind and solar-powered autonomous surface vehicle (WASP) for oceanographic measurements. This thesis presents the general design scheme, detailed aerodynamic and hydrodynamic aspects, sailing performance theory, and dynamic performance validation measurements obtained from a series of experiments. The WASP consists of a 4.2 meter long sailboat hull, a low-Reynolds number composite wing, a 2000 Watt-hour battery reservoir, a system of control actuators, a control system running on an embedded microprocessor, a suite of oceanographic sensors, and power regeneration from solar energy. The vehicle has a maximum speed of five knots and weighs approximately 350 kilograms. Results from four oceanographic missions that were conducted in the Port Everglades Intracoastal Waterway in Dania Beach Florida are presented. Water temperature, salinity and oxidation-reduction measurements recorded during these missions are also discussed.

The combination of a mono-hull and solid wing in an autonomous system is a viable design for a long-range ocean observation platform. The results of four near-shore ocean observation missions illustrate the initial capabilities of the design. Future work aimed to further reduce both the mass of the wing design and the power requirements of the system will increase performance in all operating conditions and should be considered. Furthermore, the progression of the legal framework related to ocean vehicles must be pursued with respect to unmanned autonomous systems.

ACKNOWLEDGEMENT

Dr. Karl von Ellenrieder gave me the opportunity to pursue this project, the freedom to influence its direction and the continued guidance to finish it on time.

This work could not have happened without the immense efforts of the 2007-2008 FAU senior design class. Thank you Christian Baker, Jason Engel, Dylan Kee-Manon, Anna Leland, Patricia Nault, Matt Padgett, Stewart Smith, Chris Vinci, and Chris Williams for all of your hard work!

The sea trials for this project required substantial manpower. Special thanks to Tom Furfaro, Jeff Dusek, and Nick Muzia for their time and commitment and to Mark Smith for the generous use of his powerboat.

The control system code for the WASP was written and tested by Michael Tall. Thank you very much for your time, enthusiasm and effort. This would not have happened without you.

The concept of developing a wind-powered autonomous surface vehicle was first brought to FAU by Dr. David Palmer. Without his influence, it is unlikely this project would have left the drawing board. Thank you for your continued support.

Por ultimo, mi agradecimiento a Natalia Romero, mi amor y mi sosten en los momentos mas dificiles.

TABLE OF CONTENTS

INDEX OF FIGURES

INDEX OF NOMENCLATURE

AR - Aspect Ratio
LOA - Length Overall
D - Draft (Depth of Hull)
A - Area
FA - Freeboard
M - Mass
Fn - Froude Number
Re - Reynolds Number
g - Acceleration due to Gravity
W_L - Waterline Length
B - Beam of Hull
U - Velocity
A_F - Area of Foretriangle
A_M - Area of Mainsail
C_L - Coefficient of Lift
C_D - Coefficient of Drag
β - Apparent Wind Angle
α - Aerodynamic Angle of Attack
θ - Aerodynamic Net Force Angle
ρ - Density
υ - Kinematic Viscosity
F_{Net} - Total Aerodynamic Force
F_{AD} - Aerodynamic Drag Force
F_{AL} - Aerodynamic Lift Force
F_{AR} - Aerodynamic Driving Force
F_{AS} - Aerodynamic Side Force
M_{Aero} - Aerodynamic Heeling Moment
Chord - Distance from leading edge to trailing edge on lifting surface

Hazen's Model For Sail Aerodynamics
P - Mainsail Tack Height
E - Mainsail Foot Length
LPG - Longest Perpendicular Length
I - Foretriangle Height
J - Foretriangle Width
A_{Total} - Total Sail Area
A_M - Mainsail Area
A_F - Area of Foretriangle
C_{LSail} - Total Coefficient of Lift
C_{LM} - Mainsail Coefficient of Lift
C_{LJ} - Jib Coefficient of Lift
C_{DP} - Total Coefficient of Viscous Drag
C_{DPM} - Mainsail Coefficient of Viscous Drag
C_{DPJ} - Jib Coefficient of Viscous Drag
C_{DL} - Coefficient of Induced Drag
C_{DO} - Coefficient of Mast & Topside Drag
FA - Average Freeboard
EHM - Mast Height Above Shear
EMDC - Mast Diameter
B_{Max} - Max Beam

1 Introduction

Currently there is no practical solution for long-range ocean surface observation platforms beyond passive buoy designs. Controllable platforms exist in the form of manned ships and are only available to well funded research groups. Due to the large scale of the observation area, it is important to increase accessibility to as much of the scientific community as possible. The aim of this research is to develop technology and methods that will help provide long-range sea surface platforms to scientists, researchers, and educators who would not otherwise have accessibility.

On September 20, 2004 the U.S. Commission on Ocean Policy released a document outlining its recommendations for a new national ocean policy known as the "Ocean Blueprint for the 21st Century." In response to the Commission's recommendations, the Bush Administration submitted a formal proposal to congress in the form of the U.S Ocean Action Plan in December 2004. The Plan was approved shortly after along with other substantial objectives. The Plan calls for the development of an integrated ocean observation system. An ocean observation system is a network of people, ships, sensors, satellites and other forms of technology used to monitor and develop a greater

understanding of the ocean environment. The U.S Ocean Action Plan states as one of its primary objectives to

"Build a Global earth Observation Network, Including Integrated Ocean Observation. The United States is playing a lead role in bringing the international community together to develop an integrated, comprehensive, and sustained global earth observing system of systems that includes a substantial ocean component, known as the Global Ocean Observing System (GOOS). The U.S. Integrated Ocean Observing System we be a major element of GOOS." [1]

The U.S. contribution to the GOOS exists as the U.S. Integrated Earth Observation System (IEOS). The oceans and coastal component of the IEOS is known as the Integrated Ocean Observing System (IOOS). The purpose of the IOOS is to create a fully integrated observation system that serves seven defined societal goals. The primary goal is to,

> "Efficiently link observations, data communications and management, and data analysis and modeling to form an "end-to-end" system" [2]

Creating an efficient ocean observation system, both physically and financially is one of the most significant challenges. Increasing exploration and subsequent data acquisition within the economic constraints of the modern day requires less dependency on large surface vessels and more reliance on autonomous systems. The design and implementation of Autonomous Underwater Vehicles (AUV) for example, has extended the limits of exploration while preserving safety by keeping operators out of harm's way.

Furthermore, low energy designs have extended mission length significantly. It is unquestionable that future systems will rely on autonomous vehicles, creating the need for various designs.

The IOOS currently implements the following observation platforms

- Manned Surface Vessels (Ships)
- Manned & Unmanned Aerial Vehicles (Planes, Satellites)
- Tethered & Lagrangian Drifting Buoys
- Short-Range Unmanned Autonomous Underwater Vehicles (AUV)
- Long-Range Unmanned Autonomous Underwater Vehicle (Slocum Glider Figure 1-1)

Figure 1-1 Slocum Glider AUV [3]

The Slocum Glider has made an impact on the integrated system. A glider is capable of conducting underwater observation and profiling for months at a time. A glider can record sea temperatures, current velocities, ocean depths and a variety of other measurements, but can only transmit data while immobilized on the surface. Buoys can house similar observation sensors and provide greater data transmission capabilities, but are limited for targeted and adaptive sampling due to their immobility. Aerial vehicles

provide atmospheric data quickly, often times related to meteorological events such as hurricanes. Short-range underwater vehicles provide detailed exploration of features, whether natural phenomena or underwater technology. Despite its functionality, the current IOOS system suffers from large energy and manpower consumption.

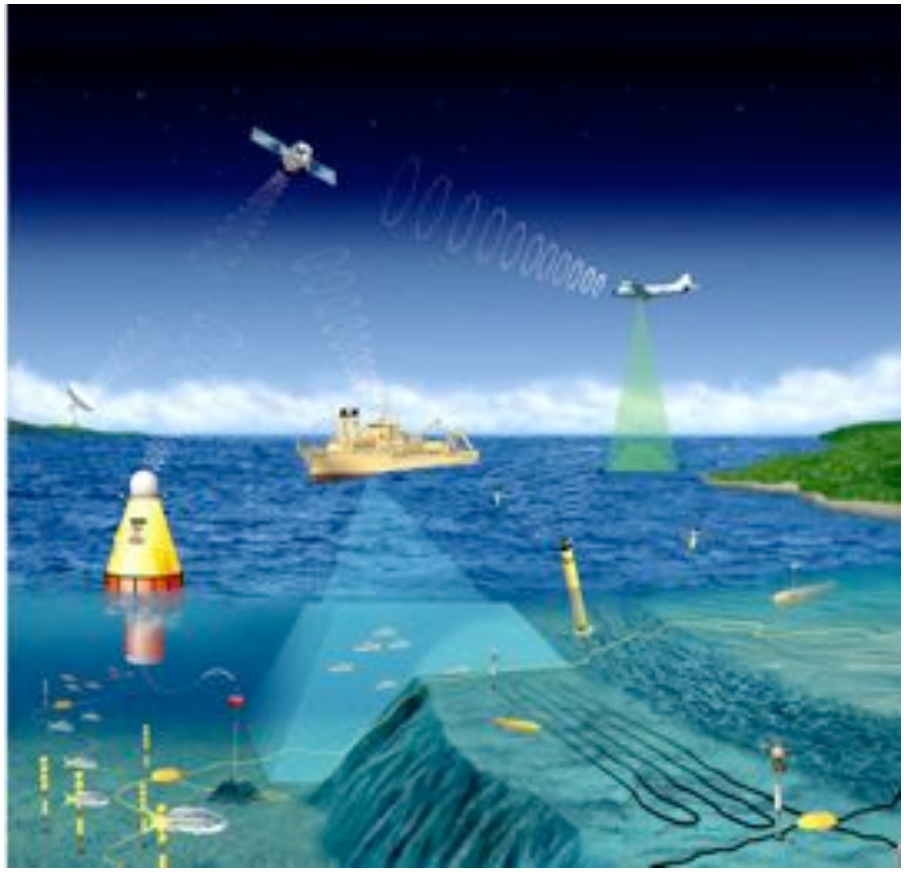

Figure 1-2 IOOS System Diagram [2]

Considering the IOOS system (Figure 1-2), it is clear that a surface equivalent to the Slocum Glider would be advantageous. A Long-Range Unmanned Autonomous Surface Vehicle would be capable of delivering a wealth of information to a globally integrated observation system. Harvesting an efficient and reliable energy source is the primary consideration for any long-range vehicle. Wind and solar energy are obvious choices, and lead to the concept of a Wind-Powered Surface Vehicle (WASP).

1.1 WIND-POWERED AUTONOMOUS VEHICLES

Although there have been numerous efforts developing wind-powered autonomous surface vehicles, there are three examples that exemplify the range of work. In 1958, the Radio Corporation of America (RCA) developed a Station Keeping Autonomous Mobile Platform (SKAMP). As seen in Figure 1-3, the platform utilizes a solid wing design and buoy like submerged body. Detailed performance results of the vehicle were not found and history of its deployments are unclear.

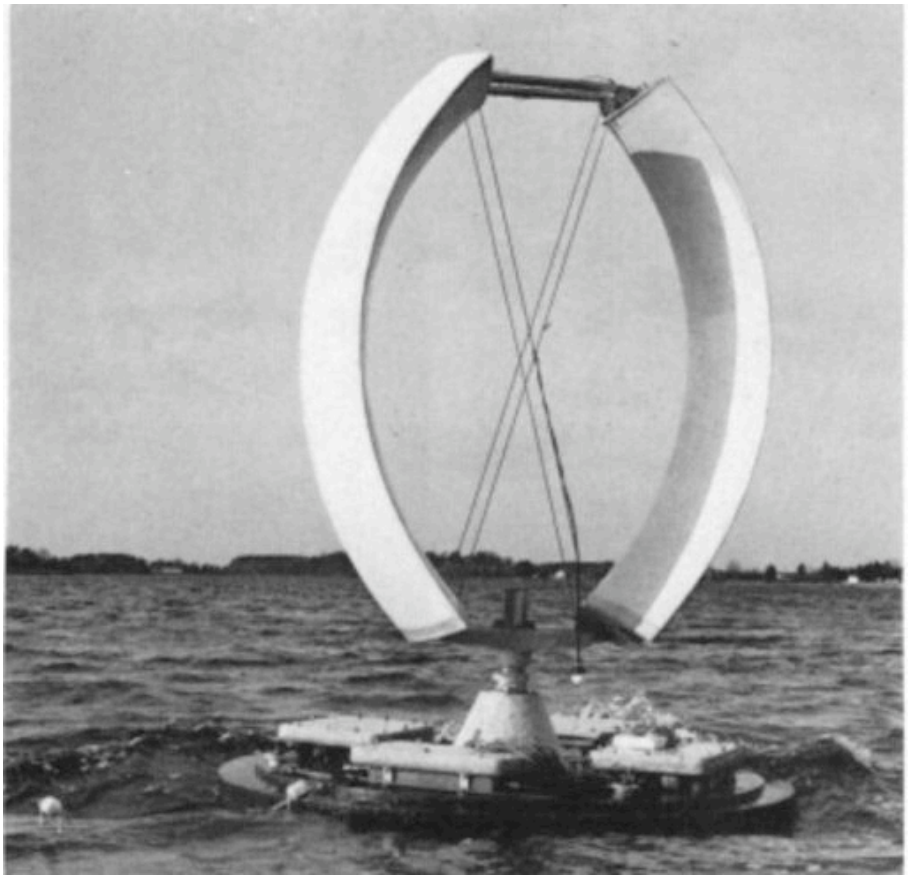

Figure 1-3 The RCA SKAMP Project [4]

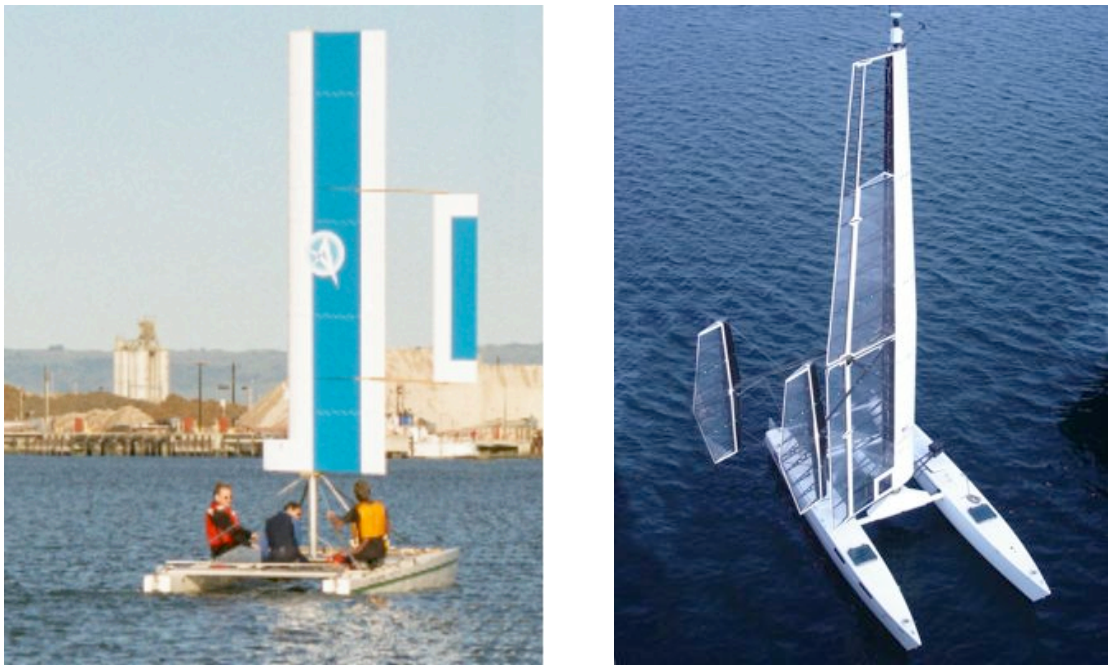

Figure 1-4 The Atlantis Project & Harbor Wing Technologies X1 Prototype [5][6]

In the early 2000's, Gabriel Elkaim developed a wing sail catamaran (Figure 1-4) while at Stanford University. The project was extremely well documented and served as an important reference in development of the WASP. A catamaran, although very stable in a calm sea state, would not be suitable for long-range open ocean deployments and served as motivation to design a monohull configuration. Multihull configurations are stable due to their large beam, but are not self-righting while capsized. For long-term observations in an open ocean environment, the probability of a capsize is very high. A second version of the catamaran was developed by Harbor Wing Technologies Inc. primarily as a port surveillance tool (Figure 1-4).

Around the same time as the Atlantis Project, a group from Aberystwyth University (UK) led by Dr. Mark Neal (Figure 1-6) organized a sailing regatta between autonomous sailboats called the Microtransat. The ultimate goal is to promote a transatlantic crossing by a wind-powered ASV. Competitions were held in 2006-2008

(Figure 1-5), and an Atlantic crossing attempt is scheduled for late 2009. Increasing the focus on ocean observation in the Microtransat race might be beneficial. Instead of focusing primarily on racing, entrants could be given incentive to collect oceanographic data during the competition.

Figure 1-5 Three Competitors preparing for the Microtransat [7]

Figure 1-6 The University of Aberystwyth 2007 Microtransat Entry [8]

1.2 WING SAIL HISTORY

Wing sails are relatively new to the sailing world, but the technology of their design is well founded through the development of airplanes. In the 1988 Americas Cup Dennis Connor and his syndicate designed and raced a catamaran with a solid wing sail (Figure 1-7). For many it marked the first time a solid wing had been seen on a high performance yacht. In the years following, wing sails were included in a variety of designs, mostly isolated to speed racing **(**Figure 1-8). For the average sailor, however a wing sail is often not worth the hassle. The most notable difficulty with wing sails is human control. Sailors rely on visual input from the sail to know if they are trimming it

properly. Wing sails do not change shape, and subsequently are extremely difficult to adjust visually.

Figure 1-7 Stars & Stripes Wing [9]

Figure 1-8 "Little Americas Cup" Rhode Island 2004 [10]

1.3 SYSTEM CONFIGURATION

The final configuration of the WASP is shown in Figure 1-9 An auxiliary propulsion system consisting of an electric motor and foldable

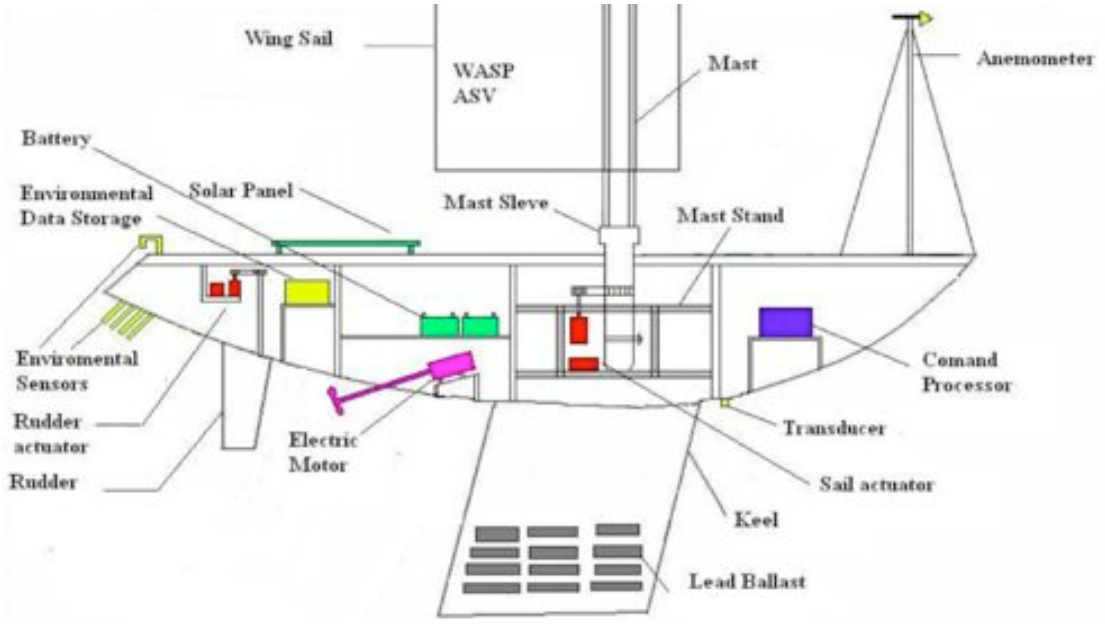

Figure 1-9 WASP System Diagram [21]

carbon fiber propeller is included for low wind conditions. A 50-Watt solar panel is used to demonstrate the concept of harvesting solar energy, but was not used during experiments. The final configuration during sea trials is shown in Figure 1-10.

Figure 1-10 WASP Final Configuration

1.4 THESIS CONTRIBUTION

The primary contribution of this thesis is to build upon previous research to better address the solution for long-range autonomous surface vehicles for oceanographic research. Specifically, the approach combines the aerodynamic efficiency of a composite

wing with the self-righting capabilities of a mono hull sailboat for use in an autonomous system. It is the belief of the author that this configuration could lead to viable solutions for acquiring oceanographic data over the long term, and will serve as a stepping-stone for future efforts. The body of this thesis will cover the methodology and design approach, numeric modeling and outline the results of initial testing.

2 Approach & Methodology

The hull of the WASP prototype was selected within the constraints of time, budget, performance, and adaptability. With an initial project schedule limited to twelve months, designing a custom hull was not feasible. Amongst existing hull designs are three distinct types: dinghies, multi-hulls, and keelboats. Dinghies (Figure 2-2) are designed with either a centerboard or dagger board configuration, and require human balance to stay upright. As an autonomous vehicle, a weighted keel would need to be added to ensure stability. Multi-hulls (Figure 2-1) are inherently stable at low angles of roll, but can capsize and are equally stable upside down, making them difficult to right. Keelboats (Figure 2-3) are generally the slowest of the three designs, but benefit from upright stability and a self-righting moment across nearly all angles of roll. A keelboat was selected as the best choice since it would require little modification and is a self-righting design.

Figure 2-1 Catamaran Designs are stable upside down and difficult to right [11]

Figure 2-2 Dinghies are light and fast but require constant human leverage to stay upright, as demonstrated here by 2008 US Olympic Gold Medalist Anna Tunnicliffe. [12]

Figure 2-3 A monohull keelboat is self-righting and modern designs have broadened the speed range beyond Froude numbers of 0.45 [13]

Figure 2-4 2.4 Meter Class Sailboat [14]

2.1 THE 2.4 METER CLASS SAILBOAT

A Sodengran 2.4 Meter Class Sailboat hull is used as the WASP platform (Figure 2-4). The hull form is a single-handed keelboat designed for ease of use and accessibility. The hull is a displacement vessel with a length overall of 4.2 meters, a beam of 0.8 meters, a draft of 1 meter, and a displacement of approximately 50 kilograms (bare hull). The design has been active in the sailing community since 1986, and knowledge of its performance is available. CAD hull lines (Figure 2-5) were provided by Swedish designer Hasse Malmsten, and are used for modeling performance characteristics such as the roll stability in Figure 2-6. Modeling provides insight for design modifications and their effect on parameters such as the center of gravity, center of buoyancy, wetted surface area, et cetera.

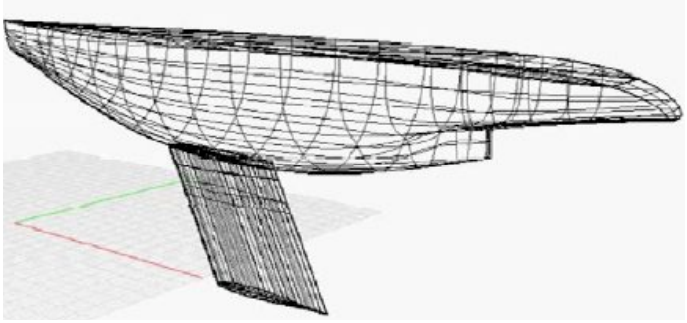

Figure 2-5 C.A.D representation of 2.4 Meter Hull

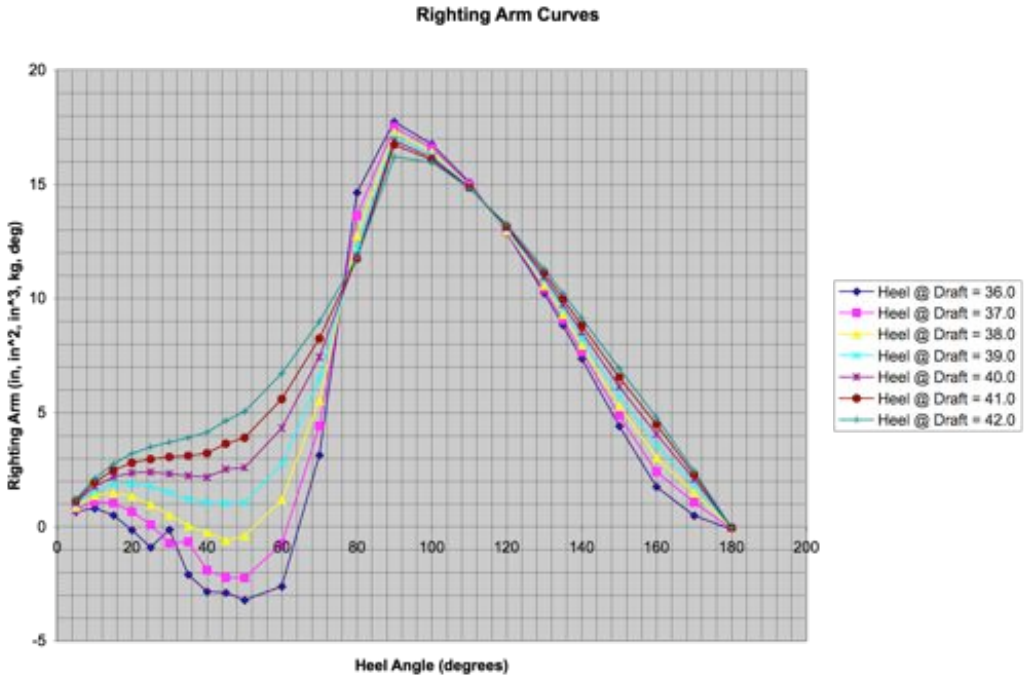

Figure 2-6 The roll stability plot suggests a region of equilibrium around 45 degrees. The plot also shows that increased loading (correlating to a deeper draft) increases the overall stability in roll.

2.2 LEAD POSITION

On a simplified level, the motion of a sailboat results from the balance of aerodynamic and hydrodynamic forces. Lead is a term used to describe the projected

distance on the hulls centerline axis between the net aerodynamic force from the sails and the net hydrodynamic force from the submerged body. The positions of the net aerodynamic and hydrodynamic forces are called the Aerodynamic and Hydrodynamic Centers of Effort, or ACE and HCE. When these forces fall in line with each other, corresponding to zero lead, the boat is balanced and no yaw moment is induced. When the forces are misaligned, corresponding to a non-zero lead, a yaw moment is induced. Most sailboats are designed with slightly negative lead; the projected ACE on the centerline axis falls behind the projected HCE. This creates a small yawing moment that will turn the boat into the wind. Such a yawing moment is preferred in strong wind conditions, as the hull will naturally de-power itself by turning into the wind.

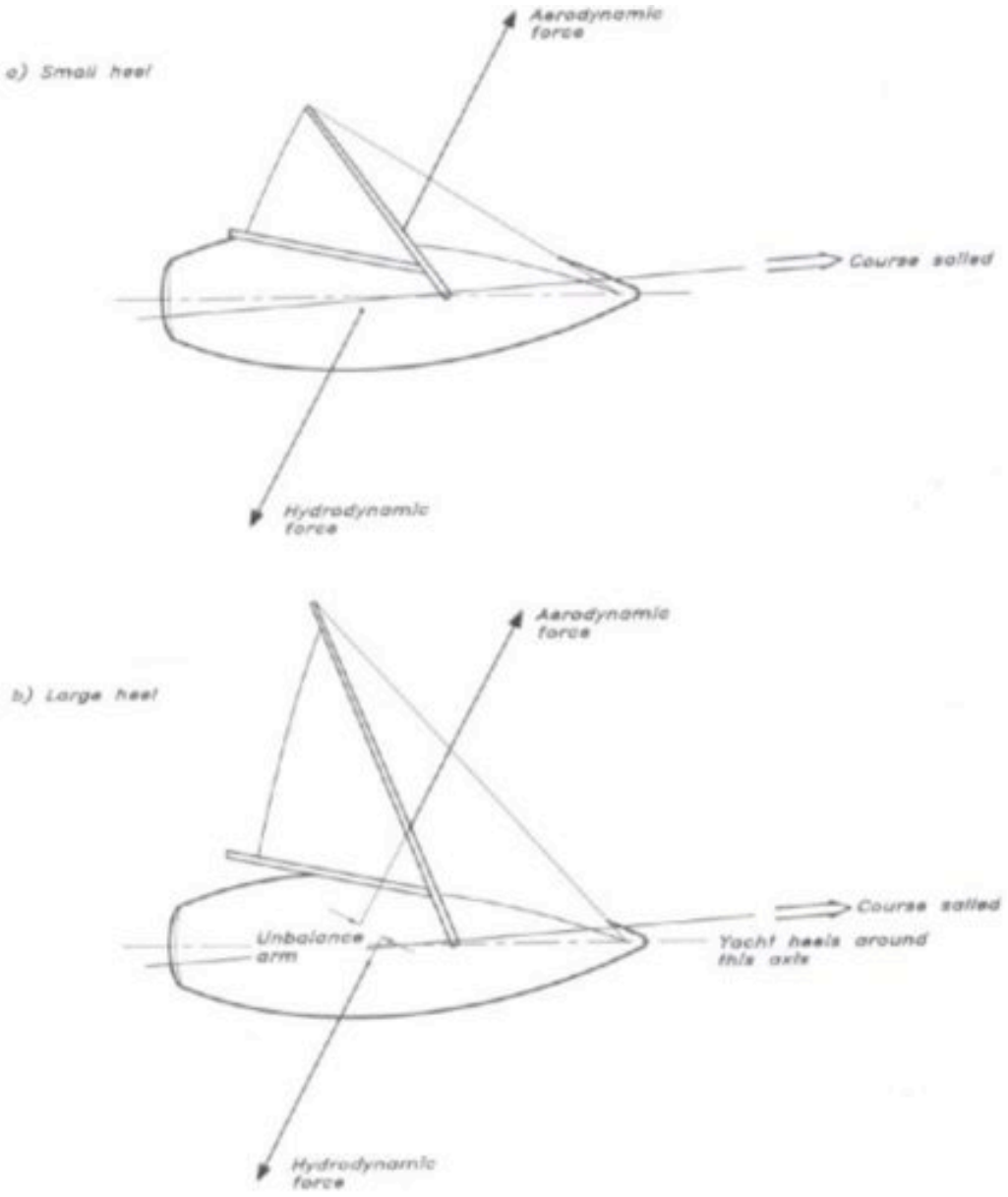

Figure 2-7 The effect of large roll angles on lead. [15]

Knowing the designed lead of the original two-cloth sail system is necessary for proper placement of the mast of a new sail configuration. The author determined the location of the ACE using a geometric technique commonly used within the sailboat

racing community and outlined in sailing literature [13] with a set of racing sails provided by Canadian Olympic hopeful Bruce Millar.

Figure 2-8 The author finding the Aerodynamic Center of Effort for the cloth sail configuration of the 2.4 Meter Class Sailboat

Figure 2-9 YD-40 Lead Calculation Diagram and Field Notes [15]

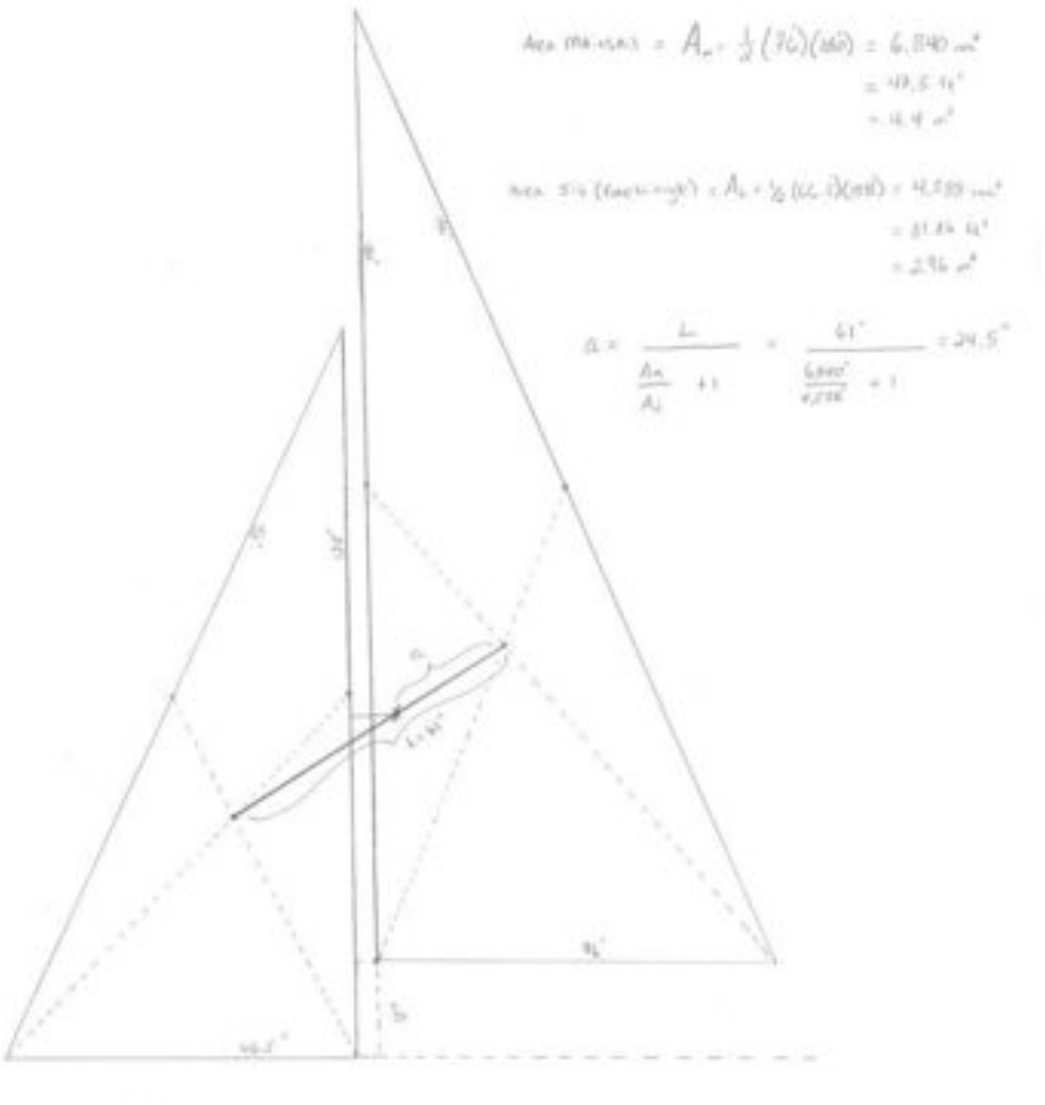

Figure 2-9 YD-40 Lead Calculation Diagram and Field Notes [15]

2.3 WIND PROPULSION

Wind powered propulsion is proven in the sport of sailing in the form of cloth sails. Sails serve the same purpose as wings but rarely achieve equivalent levels of aerodynamic performance. A properly designed wing would have a higher coefficient of

lift and significantly smaller coefficient of drag. To a trained sailor, a sail is easily tuned and controlled. If it is trimmed at too small an angle of attack, the pressure gradient becomes too small to maintain the shape of the cloth and is visible as a "luffing" sail. Wings, on the other hand, can be difficult for a human to control, as there are no visual signs of improper trim. From the perspective of an automated system, the ability to visualize anything is less important, since feedback is acquired from non-visual sensors. Solid wings can be controlled on a freestanding rotating mast while sails require complicated rigging systems to control the shape of the sail. Furthermore, the durability of a sail is not appropriate for long-term offshore missions or tropical storm strength wind conditions. A solid wing, although more complicated to design, is the best choice. [21]

2.4 FUNDAMENTAL AERODYNAMICS

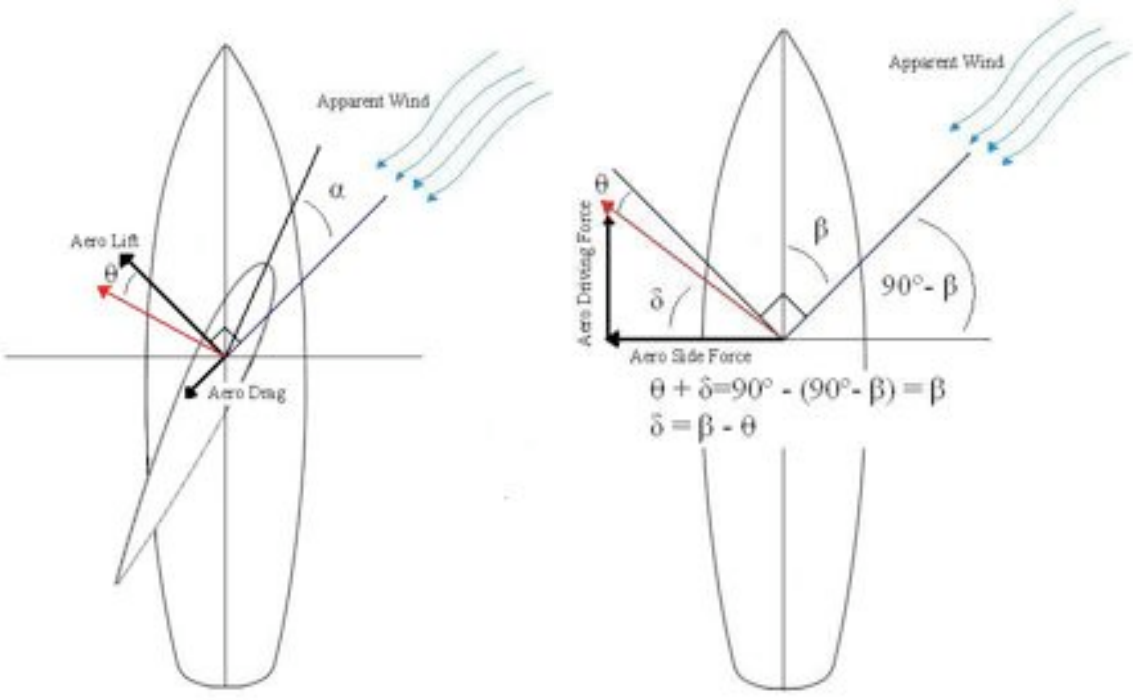

Figure 2-10 Sailboat Aerodynamic Free Body Diagram

An angled lifting surface creates two distinct forces when exposed to a fluid in motion. Lift is generated perpendicular to the free stream velocity while drag acts in the same direction (Figure 2-10). The magnitude of each force is defined in EQ 2-1.

$C_L = Lift\ Coefficient,\ C_D = Drag\ Coefficient$
$\rho = Density\ of\ Air$
$U = Apparent\ Wind\ Velocity$
$A = Area\ of\ Wing$

$$F_{AL} = \frac{1}{2} C_L \rho U^2 A$$

$$F_{AD} = \frac{1}{2} C_D \rho U^2 A$$

EQ 2-1

Referring to Figure 2-10, the lift and drag forces are combined into a single net aerodynamic force whose magnitude and angle relative to the free stream perpendicular are defined in EQ 2-2.

$$F_{net} = \sqrt{(\frac{1}{2} C_L \rho U^2 A)^2 + (\frac{1}{2} C_D \rho U^2 A)^2}$$

$$= \sqrt{(\frac{1}{4} \rho^2 U^4 A^2)(C_L{}^2 + C_D{}^2)}$$

$$Tan(\theta) = \frac{F_{AD}}{F_{AL}} = \frac{\frac{1}{2} C_D \rho U^2 A}{\frac{1}{2} C_L \rho U^2 A} = \frac{C_D}{C_L}$$

$$\theta = Tan^{-1}(\frac{C_D}{C_L})$$

EQ 2-2

The net aerodynamic force exerted by the lifting surface can be expressed as two distinct forces on a sailboat hull. The component parallel to the direction of motion is the Aerodynamic Driving Force (F_{AR}), while that perpendicular is the Aerodynamic Side Force (F_{AS}). Besides being a function of the angle of attack of the wing (α), both

F_{AR} & F_{AS} are dependent on the apparent wind angle (β). F_{AR} & F_{AS} are visualized in Figure 2-10 and defined in EQ 2-3.

$$\theta + \delta = 90^{\circ} - (90^{\circ} - \beta) = \beta$$
$$\delta = \beta - \theta$$
$$F_{AR} = F_{net}\sin(\beta-\theta) = \sin(\beta-\theta)\sqrt{(\frac{1}{4}\rho^2 U^4 A^2)(C_L{}^2 + C_D{}^2)} \qquad \textbf{EQ 2-3}$$
$$F_{AS} = F_{net}\cos(\beta-\theta) = \cos(\beta-\theta)\sqrt{(\frac{1}{4}\rho^2 U^4 A^2)(C_L{}^2 + C_D{}^2)}$$

Equation 2-3 holds true for any lifting surface, whether a solid wing or clothe sail. For optimal performance of a sailing vehicle, the lifting surface shall maximize the Aerodynamic Driving Force while minimizing the Aerodynamic Side Force. The ratio $\frac{F_{AR}}{F_{AS}}$ is at a maximum when the angle θ is minimized. The relation and respective limit are shown in EQ 2-4.

$$\frac{F_{AR}}{F_{AS}} = \frac{F_{net}\sin(\beta-\theta)}{F_{net}\cos(\beta-\theta)} = \tan(\beta-\theta)$$
$$= \tan(\beta - \tan^{-1}(\frac{C_D}{C_L}))$$
$$for\ 0 \le \beta \le 180^{\circ} \qquad \textbf{EQ 2-4}$$
$$\lim_{C_L \to \infty} \tan(\beta - \tan^{-1}(\frac{C_D}{C_L})) = \tan(\beta)$$

2.5 AIRFOIL DESIGN

It has already been discussed qualitatively that a solid wing offers better controllability and robustness then a cloth sail, but its aerodynamic performance is

equally important. The first step in designing a wing is selecting the two-dimensional airfoil section. Using the airfoil analysis software XFOIL, the performance of a variety of airfoil sections can be compared and optimized. The WASP section must be symmetrical since the craft must generate lift on both tacks. A Reynolds Number approximation of $\mathrm{Re} = 229{,}000$ is used for initial iterations (7 knots true wind @ sea level in EQ 2-5) as that is the projected operating condition and is comparable to similar past efforts found in published literature [5].

$$\mathrm{Re} = \frac{UL}{\nu}$$
$$U = Wind\ Velocity = 7\ [knots] = 3.6\ [\mathrm{m/s}]$$
$$L = Chord\ Length = 1\ [m]$$
$$\nu = 1.57 \times 10^{-5}\ [\mathrm{m}^2 / s] \qquad \textbf{EQ 2-5}$$
$$\mathrm{Re} \approx 229{,}000$$
$$note: \nu @ T = 25\ [^{\circ}C]$$

Particular attention is placed on the sections method of separation and stall at high angles of attack. Separation from the leading edge results in an immediate disturbance in the downstream flow [16], which is difficult to predict or control. Separation initiating off the trailing edge is preferred since it evolves more gradually. Overall the section is not designed for perfection, rather as a conservative design choice with strong overall performance.

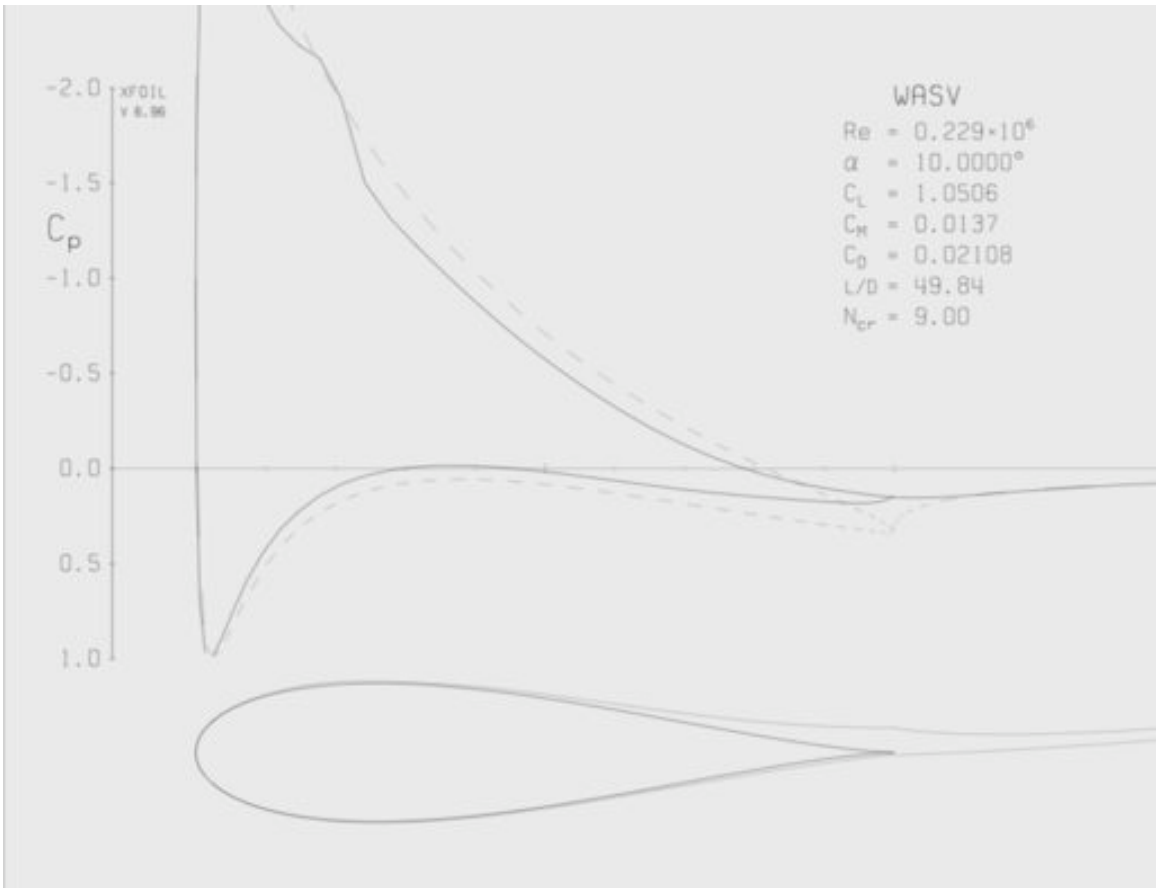

Figure 2-11 WASV Wing Polar Plot (XFOIL)

WASV
Re = 0.229×10⁶
α = 10.0000°
CL = 1.0506
CM = 0.0137
CD = 0.02108
L/D = 49.84
Ncr = 9.00

Figure 2-12 Polar Data

The Xfoil viscous calculation provides a two dimensional analysis of the airfoil (Figure 2-11). For simplicity the three-dimensional coefficient of lift is assumed to be

equal to the two-dimensional model [17]. The same approximation however is not made for the drag coefficient. Two-dimensional analysis does not consider the effect of induced drag, namely that caused by pressure differences across the wing surface that induce a "spillage effect" across the wing tip, and resulting vortex. The three dimensional coefficient of drag is approximated by adding the two dimensional coefficient from Xfoil with an induced drag component that is calculated using Lifting Line Theory (EQ 2-6)[13]. Figure 2-13 shows how an increased aspect ratio will reduce the induced drag coefficient and increase the lift coefficient for an angle of attack of ten degrees.

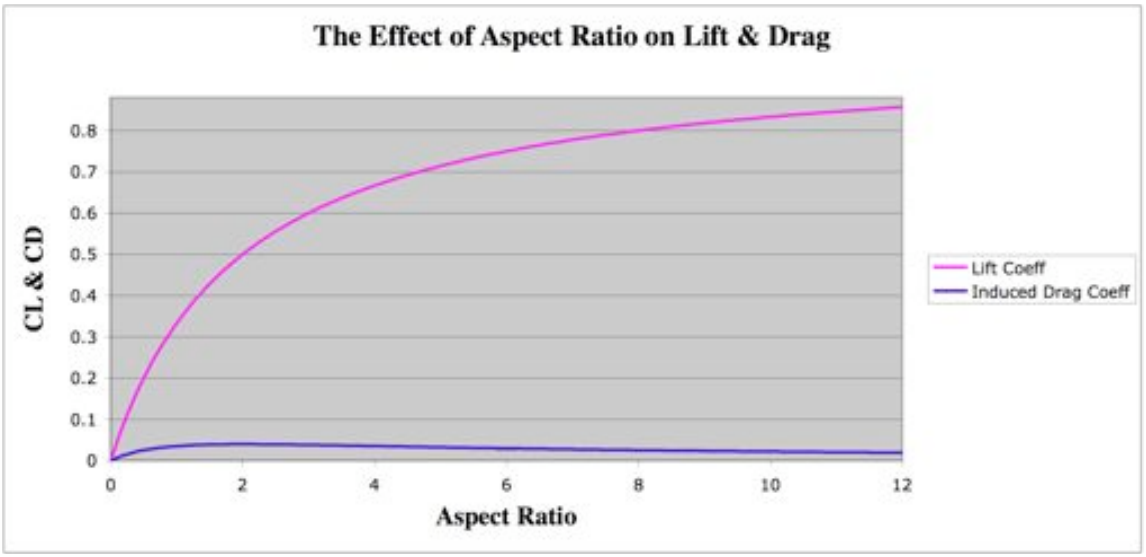

Figure 2-13 Effect of Aspect Ratio

$$C_D = C_d + C_{Di}$$
$$C_d = 2D\ Drag\ (XFoil)$$
$$Induced\ Drag = C_{Di} = \frac{C_L{}^2}{\pi AR}$$
$$AR = \frac{b^2}{A} = \frac{25\ [\mathrm{m}^2]}{5\ [\mathrm{m}^2]} = 5$$
$$C_{Di} = 0.07$$
$$C_D = 0.021 + 0.07 = 0.091$$

EQ 2-6

The designed airfoil has a maximum thickness of 20% the chord length. Maximum thickness occurs at 25% of the chord length from the leading edge. Figure 2-11 shows a maximum pressure achieved within the first 10% of the chord. The pressure immediately begins its recovery along the entire section. Separation is a concern with any low Reynolds number airfoil, and is assumed to occur. Instead of designing to prevent separation and stall, the WASP section is designed to maintain solid performance across a variety of angles of attack without any drastic aerodynamic performance changes. XFOIL analysis does not suggest separation will occur until an approximate angle of attack of fifteen degrees. This prediction is a result of analyzing the streamlines of the foil in two-dimensional viscous flow and checking for visibly separated regions. For this foil, flow separation initiates off the trailing edge. Analysis of the ratio $\frac{F_{AR}}{F_{AS}}$ for the above section along with two modified sections for angles of attack between five and fifteen degrees is shown in Figure 2-14.

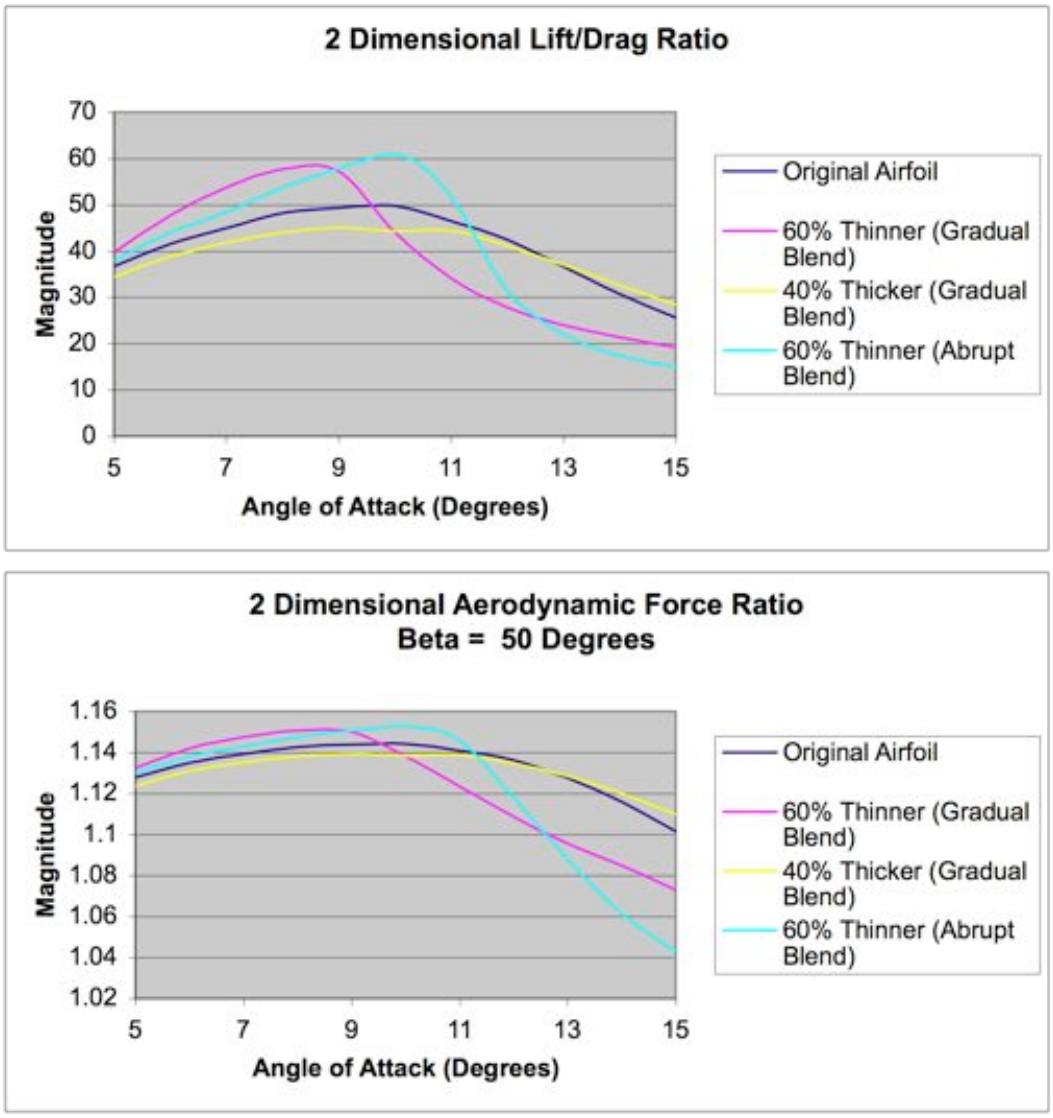

Figure 2-14 F_{AR} / F_{AS} Variation Plot - The effect of leading edge modification on airfoil performance in two-dimensional viscous flow. Note that the position and magnitude of the maximum thickness of each airfoil is the same.

In order to achieve large lift coefficients, symmetric low Reynolds number airfoils must be very thick (a baseline of 15-20% is common). Modifying the nose and streamlining it into the base section shape can affect the pressure distribution, the lift to drag ratio, and the general flow characteristics. Two modifications are shown in Figure 2-14. A thin nose variation results from optimizing based on maximizing the lift coefficient

and the lift/drag ratio. This also correlates to a higher maximum achieved aerodynamic force ratio but also to a more rapid decline at angles of attack slightly larger then optimal. From the point of view of a WASP, this is highly undesirable. When the WASP encounters an apparent wind shift caused by sea surface or atmospheric phenomena, the control system will not likely be capable of instantly adjusting the trim angle. It is notable to mention that research has shown that the rate of change of angle of attack does not affect the angle at which separation begins [18]. This is an important factor in developing the wing control system. Overall, it must be expected that the wing will operate within a range of angles of attack, making narrow nose variations a poor choice. Figure 2-14 suggests that increasing the nose thickness improves the upper end angles of attack performance, but decreases the lower angle of attack performance. The trend shows that a thicker nose section makes the aerodynamic force ratio "flatten" out. A flat aerodynamic ratio response over the angle of attacks of interest is optimal for a conservative design choice.

2.6 HAZEN'S MODEL OF CLOTH SAIL AERODYNAMICS

In order to compare performance between a cloth sail and solid wing, the existing cloth sail design of the 2.4 Meter Sailboat must be examined. G. Hazen developed an aerodynamic model for sailing yachts in 1980 [15], which quickly became the backbone of many velocity prediction programs (VPP). The model presents the three-dimensional coefficients of lift and drag as functions of apparent wind angle. The angle of attack of

the sail is not included, but assumed set for optimal performance. Following Hazen's model with the parameters of the 2.4 Meter Sailboat produces EQ 2-7 through 2-11 for an apparent wind angle of 50 degrees [15].

$$A_{Total} = A_F + A_M$$

$$Coefficient\ of\ Lift = C_{LSail} = \frac{C_{LM}A_M + C_{LJ}A_J}{A_{Total}}$$

$$C_{LM} = 1.5 @ \beta = 50^o = Apparent\ Wind\ Angle \qquad \textbf{EQ 2-7}$$

$$C_{LJ} = 0.5 @ \beta = 50^o$$

$$C_{LSail} = 1.056$$

$$Coefficient\ of\ Viscous\ Drag = C_{DP} = \frac{C_{DPM}A_M + C_{DPJ}A_J}{A_{Total}}$$

$$\mathrm{C_{DPM}} = 0.15 @ \beta = 50^o \qquad \textbf{EQ 2-8}$$

$$C_{DPJ} = 0.25 @ \beta = 50^o$$

$$C_{DP} = .194$$

$$Coefficient\ of\ Induced\ Drag = C_{DL} = C_L^2 \cdot (\frac{1}{\pi \cdot AR} + 0.005)$$

where

$$AR = \frac{(1.1 \cdot (EHM + FA))^2}{A_T} \qquad \textbf{EQ 2-9}$$

$$AR = 3.8$$

$$C_{DL} = .099$$

$$Coefficient\ of\ Mast\ /\ TopSideDrag = C_{DO}$$

$$C1.13 \cdot \frac{(B_{Max}FA) + (EHM \cdot EMDC)}{A_T} \qquad \textbf{EQ 2-10}$$

$$C_{DO} = .0661$$

$$Total\ Drag = C_{DSail} = C_{DP} + C_{DL} + C_{DO} \qquad \textbf{EQ 2-11}$$

$$C_{DSail} = 0.194 + 0.099 + 0.0661 = 0.3591$$

2.7 SAIL VS. WING

The aerodynamic performance of cloth sails is satisfactory for a WASP. As stated before, the downfall of cloth sails are poor durability and controllability in an autonomous system. Using the parameters defined by Hazen's Model, the aerodynamic efficiency of the cloth sails is determined based on its achieved aerodynamic ratio compared to the maximum possible value at an apparent wind angle of 50 degrees (EQ 2-12).

$$C_L \approx 1.056 \quad C_D \approx 0.3591 \quad \beta = 50^\circ$$
$$\frac{F_{AR}}{F_{AS}} = \tan(50^\circ - \tan^{-1}(.34)) = 0.606$$
$$\frac{F_{AR}}{F_{AS}} Max = \tan(50^\circ) = 1.192 \qquad \textbf{EQ 2-12}$$
$$Cloth\ Sail\ Efficiency = 50.08\%$$

The aerodynamic performance of a solid wing sail is analyzed using the airfoil software XFOIL. A Reynolds number approximation of 229,000 is chosen to determine the viscous solution for apparent wind strength of seven knots. The aerodynamic force ratio decreases linearly with increasing angle of attack. This is due to the increasing effect of induced resistance. The wing is analyzed at an angle of attack of 10 degrees, approximately the largest angle before separation is expected to occur, and represents an average performance condition.

$$C_L \approx 1.0506 \quad C_D \approx 0.091 \; \beta = 50^\circ$$
$$\frac{F_{AR}}{F_{AS}} = \tan(50^\circ - \tan^{-1}(0.0866)) = 1.002$$
$$\frac{F_{AR}}{F_{AS}} Max = \tan(50^\circ) = 1.192 \qquad \textbf{EQ 2-13}$$
$$Solid\ Wing\ Sail\ Efficiency = 84\%$$

From EQ 2-12 and EQ 2-13 it is clear that both the coefficients of lift and drag play an equal role in maximizing the efficiency of a lifting surface. It is a common misinterpretation that wings provide more lift then cloth sails. In fact, the lift coefficients of symmetric wings and modern cambered cloth sails are typically similar, with the later often notably greater. Wings however benefit from significantly smaller drag coefficients, and their resulting high efficiency is a result of that characteristic.

3 Wing Design

Combining a mono-hull with a solid wing requires strict attention to weight. Excess weight above the center of gravity of the WASP will result in an undesirable rolling moment, yet a large aspect ratio is required to minimize induced drag caused by "spillage affects". Reducing the weight of a composite while maintaining its strength is no easy task. Defining the minimum required surface area of the wing, its aspect ratio, and its expected moments and reaction forces, will illustrate the limitations of the design.

3.1 WING SCALING & KEEL CONSIDERATIONS

As stated before, the existing design of the Sodengran 2.4 Meter Sailboat is successfully proven. From sailors input it is clear that the sail parameters are optimal for light wind and flat conditions, while overpowering in heavy wind. The wing design shall be scaled to deliver the same driving force as the existing cloth design, while taking advantage of a smaller aerodynamic side force. This decision is based on fabricating the smallest wing possible that will deliver enough effective force to propel the boat. The scaling calculations are shown in EQ 3-1 and EQ 3-2.

Cloth Sail

$\beta = 50^\circ \quad \rho = 1.2\ [\frac{kg}{m^3}] \quad U = 3.6\ [\frac{m}{s}] \quad A \approx 9[m^2]$

$C_L \approx 1.056 \quad C_D \approx 0.3591$

$$F_{AR} = F_{net}\sin(\beta - \theta) = \sin(\beta - \tan^{-1}(\frac{C_D}{C_L}))\sqrt{(\frac{1}{4}\rho^2 U^4 A^2)(C_L{}^2 + C_D{}^2)} \qquad \textbf{EQ 3-1}$$

$F_{AR} = 40.45\ [N]$

$$F_{AS} = F_{net}\cos(\beta - \theta) = \cos(\beta - \tan^{-1}(\frac{C_D}{C_L}))\sqrt{(\frac{1}{4}\rho^2 U^4 A^2)(C_L{}^2 + C_D{}^2)}$$

$F_{AS} = 66.76\ [N]$

Wing Sail

$\alpha = 10^\circ \quad \beta = 50^\circ \quad \rho = 1.2\ [\frac{kg}{m^3}] \quad U = 3.6\ [\frac{m}{s}] \quad A \approx 7\ [m^2]$

$C_L \approx 1.0506 \quad C_D \approx 0.091$

$$F_{AR} = F_{net}\sin(\beta - \theta) = \sin(\beta - \tan^{-1}(\frac{C_D}{C_L}))\sqrt{(\frac{1}{4}\rho^2 U^4 A^2)(C_L{}^2 + C_D{}^2)} \qquad \textbf{EQ 3-2}$$

$F_{AR} = 40.62\ [N]$

$$F_{AS} = F_{net}\cos(\beta - \theta) = \cos(\beta - \tan^{-1}(\frac{C_D}{C_L}))\sqrt{(\frac{1}{4}\rho^2 U^4 A^2)(C_L{}^2 + C_D{}^2)}$$

$F_{AS} = 40.55$ [N]

The above forces are calculated in wind conditions equivalent to a Reynolds number of 229,000, approximately seven knots apparent wind. As the wind increases, the sail area required to propel the WASP decreases. In addition, XFOIL models show that increased angles of attack will create a larger net aerodynamic force, while maintaining an acceptable aerodynamic force ratio. It is tempting to implement larger angles of attack and reduce the wing area, but it is likely that such angles of attack will suffer from separation and not perform as XFOIL predicts. It is equally significant to consider the global effect of the Aerodynamic Side Force. Referring to classic sailboat theory, the side force on a yacht is balanced by hydrodynamic forces from the keel. A keel is designed as

an underwater low speed wing. Keels are typically optimized for small angles of attack. Stalling of a keel or centerboard occurs when the aerodynamic side force on the sailboat is so large compared to the driving force that the angle of attack of water flowing over the keel is large enough to induce a separated flow [19]. This should not be an issue with the current wing design since the magnitudes of the two aerodynamic side forces are nearly equal, while the aerodynamic driving force of the wing is greater then that of the cloth sail.

3.2 FABRICATION RESTRICTIONS

Fabricating a wing with a one-sided surface area of seven square meters and an aspect ratio of at least five would require a wingspan of approximately six meters. In order to minimize weight, the wing would have to be a composite structure. The center spar, the component of the wing that supports the entire structure would need to strong, stiff and light. The best material is carbon fiber, but is extremely expensive and difficult to obtain in six-meter tubes with appropriate wall thickness. The only affordable 100% carbon spars with appropriate parameters are high-performance windsurf masts. Windsurfing masts are available in sizes up to 5.5 meters, which would restrict the wingspan to 4.5 meters (allowing proper spacing between deck and wing). Financial restrictions forced this substitution, and will make the optimal wind conditions of the final design higher than the original design conditions.

3.3 MOMENTS & REACTION FORCES

The aerodynamic side force serves as the force that creates a rolling moment, herein referred to as the aerodynamic rolling moment and illustrated in Figure 3-1.

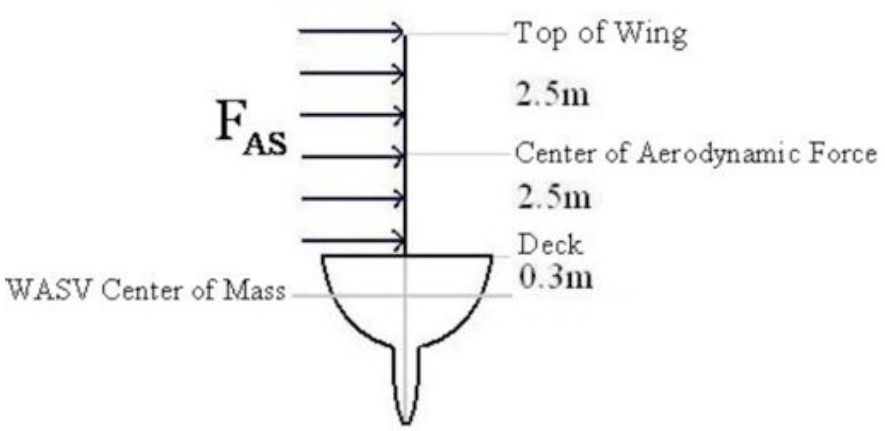

Figure 3-1 Front View Aerodynamic Heeling Moment

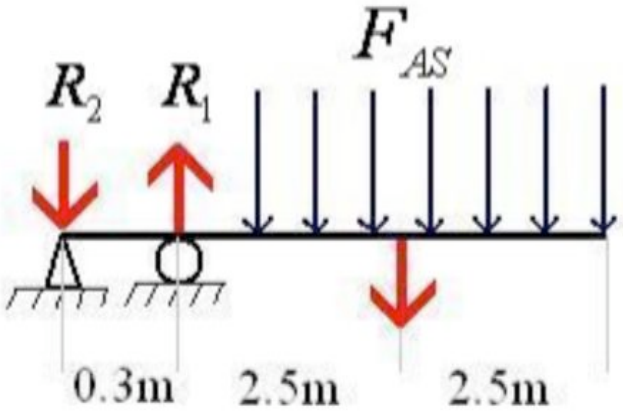

Figure 3-2 Solid Mechanics - Aerodynamic Reaction Forces

Figure 3-2 assumes a wing height of five meters, and a deck 1/3 meter above the center of gravity. The Aerodynamic side force, defined above is primarily a function of wing geometry, wind speed, and angle of attack and apparent wind angle. Assuming the wing acts as a solid beam, and that the aerodynamic force is uniformly distributed across its surface, the resultant aerodynamic moment is approximated as,

$$M_{aero} = \frac{17}{6} F_{AS} \qquad \textbf{EQ 3-3}$$

Considering a freestanding wing structure with two contact points (mast collar through the deck and mast step at base of hull), the reaction forces on the platform due to the aerodynamic side force are approximated using force and moment balance are expressed as,

$$R_1 = \frac{17}{2} F_{AS}$$

$$R_2 = \frac{15}{2} F_{AS} \qquad \textbf{EQ 3-4}$$

The directions of the forces are illustrated in Figure 3-2. These approximations are important in determining the force tolerances of the platform to avoid catastrophic failure. The weight of the wing will induce a significant gravitational moment in a state of heel. The magnitude and direction of the gravitational heeling moment is illustrated in Figure 3-3.

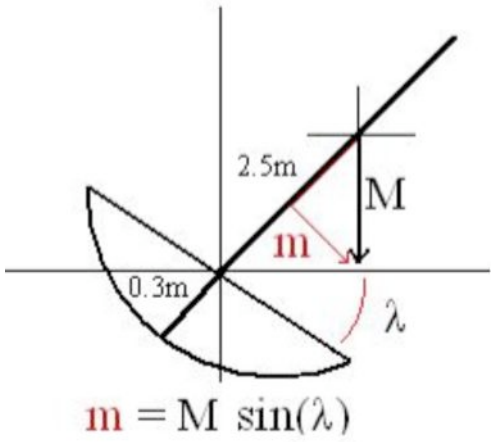

Figure 3-3 Gravitational Rolling Moment

The weight of the wing induces a larger moment as the heel angle (λ) increases towards ninety degrees (capsized). The weight of the wing combined with the aerodynamic side force creates the total heeling moment caused by the wing and resultant reaction forces,

$$M_{wing} = \frac{17}{6}(m_{wing}\sin(\lambda) + F_{AS})$$

$$R_1 = \frac{17}{2}(m_{wing}\sin(\lambda) + F_{AS}) \qquad \textbf{EQ 3-5}$$

$$R_2 = \frac{15}{2}(m_{wing}\sin(\lambda) + F_{AS})$$

3.4 WING DESIGN

With the wingspan and aspect ratio limitation outlined above, and the two dimensional airfoil section finalized, the remaining challenge would be the final assembly design and material selection. The author called upon sailboat design expert Steve Clark of Bristol, Rhode Island to offer some recommendations. Steve has been sailing and designing some of the most radical and high performance sailboats in the world, including A-Class Catamarans and International Canoes. With regards to wings, Steve worked with Team Cogito to win the 1996 & 2004 C-Class Catamaran Championship (also known as the "Little America's Cup") using a wing design.

Figure 3-4 Steve Clark & Cogito [10]

It became clear talking with Steve that in order to design and build a wing sail in eight months with a limited budget would require a simple design. The basic components of a wing sail are a main spar, cross-sectional ribs, a leading edge element, stiffening elements, and an outer impermeable membrane.

Spar – The only affordable 100% carbon spar with appropriate material specifications was the Fiberspar 6000 Reflex mast, made available at a very generous price by Fiberspar Inc. It is a tapered spar, and each rib would have to be designed accordingly.

Mast Length (cm)	550
IMCS Stiffness	36
Reflex Indicator	6000
Carbon Content	100%
Weight (kg)	2.25

Fiberspar Reflex 6000 Windsurf Mast

Ribs – The outline of each rib is defined by the airfoil geometry defined above. The rib material, thickness of each rib, the rib spacing, the total number of ribs, and additional modifications are variables of interest in the design. A primary consideration in material selection is minimizing water absorption. Two materials, marine-plywood and closed cell syntactic foam are deemed best. Using Pro-Engineer C.A.D software, a model of the master rib is analyzed. Each plywood rib is projected to weigh approximately 335 grams

(0.74 pounds), while syntactic foam rib could be as light as 135 grams (0.3 pounds). The difference may seem negligible, but for a wing with 20 ribs, using syntactic foam would immediately save nearly nine pounds of weight and reduce the gravitational rolling moment by approximately 11.3 Newton-meters. For illustrative purposes, an increase of the gravitational rolling moment by 11.3 Newton-meters would require an additional 34 kilograms (75 pounds) of counterweight in the keel to counter-balance the added weight. An additional benefit of syntactic foam is its ease of cutting in a CNC machine (Figure 3-5).

It is clear that the weight of the ribs must be minimized. Upon closer inspection of Figure 2-11, the pressure gradient between the windward and leeward sides of the wing is lowest across the last two thirds of the chord length. Reducing material in this region could help minimize overall weight while not sacrificing structural integrity. The bulk of the foam in this region should be removed.

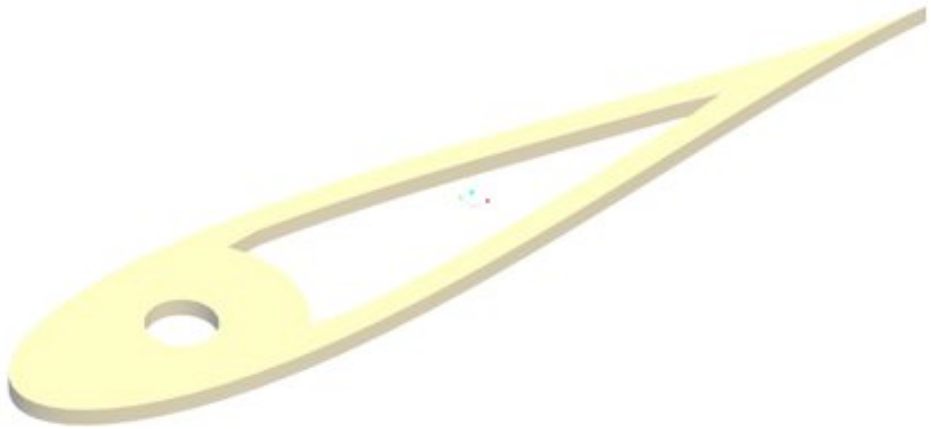

Figure 3-5 C.A.D Representation of Master Rib

Leading Edge – The leading edge element is essentially a composite shell in the shape of the leading section of the wing (Figure 3-6). Its primary purpose is to strengthen the wing by distributing tension, compression and torsion across the entire wingspan. The leading edge shell is designed to fully enclose the leading 30% of the wing, and combined with the spar and ribs provide strength and rigidity.

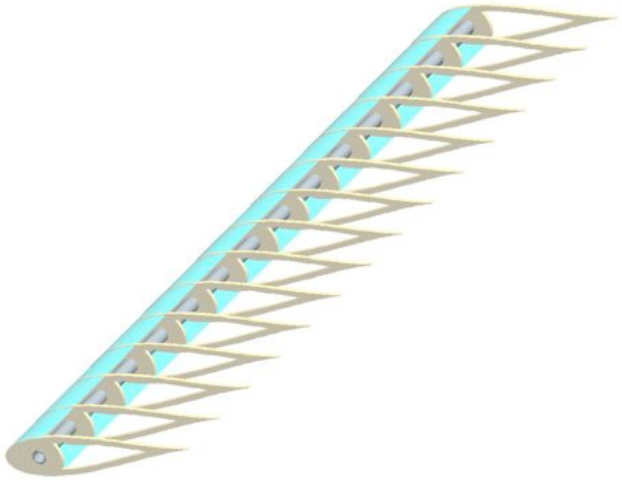

Figure 3-6 C.A.D Wing Assembly

Skin - As a skeleton, the final wing assembly will require an impermeable skin on its outer surface. A heat shrinking thermoplastic known as Monokote was initially considered, but the additional costs and complexity of its application were substantial. The final decision was to use a similar thermoplastic used in the boat storage industry. The material is robust, light, and resistant to ultraviolet light exposure for up to twelve months. Additionally, it can be applied by a professional for a low price.

3.5 WING FABRICATION

Details of the wing fabrication process can be found in Appendix A. The completed wing is shown in Figure 3-7.

Figure 3-7 Final Wing Assembly

4 Velocity Prediction Program

Developing a theoretical model to predict the velocity of the vehicle in different wind conditions can be an important step in developing a control system. Unlike propeller-powered boats, sailboat performance varies with different wind speeds and apparent wind angles. Plots of the velocity vs. apparent wind angle, known as "polars" in the sailing industry, would provide insight into the performance of the WASP. The proposed model uses steady-state approximations to predict set point conditions of the vehicle in various conditions. The approach combines Newton's second law with empirical data from sailboat research.

4.1 FORCE IDENTIFICATION

The forces are organized into categories:

I. **Aerodynamic Forces**
    a. Wing Force
        i. Wing Lift
        ii. Wing Drag
            1. Friction

2. Induced

b. Parasitic Drag

II. Hydrodynamic Forces (Lifting Surfaces)

a. Keel Force
   i. Keel Lift
   ii. Keel Drag
      1. Friction
      2. Induced

b. Rudder Force
   i. Rudder Lift
   ii. Rudder Drag
      1. Friction
      2. Induced

III. Hydrodynamic Forces (Entire Hull)

a. Viscous
   i. Friction
   ii. Viscous Pressure
   iii. Roughness

b. Residuary
   i. Wave

c. Heel

d. Added Waves

IV. Static Forces

a. Righting Forces (Those that influence the hull to stay upright)
   i. Keel Gravitational
   ii. Added Buoyancy due to Roll

b. Capsize Forces (Those that influence the hull to capsize)
   i. Wing Gravitational

Knowledge of the forces created by lifting surfaces (wing, keel and rudder) has already been explored in Section 3-1. Analysis of the static forces and their respective moments was outlined in Section 4-3. The parasitic, or topside drag represents a frictional contribution caused by equipment above the waterline. Typical sailboats have a mast,

wire stanchions, and other equipment on the deck. These configurations tend not to be aerodynamically streamlined and can contribute to parasitic drag, especially in heavy winds. Figure 4-1 illustrates how large a streamline body must be to create the equivalent drag of a tiny circular shape! [15]

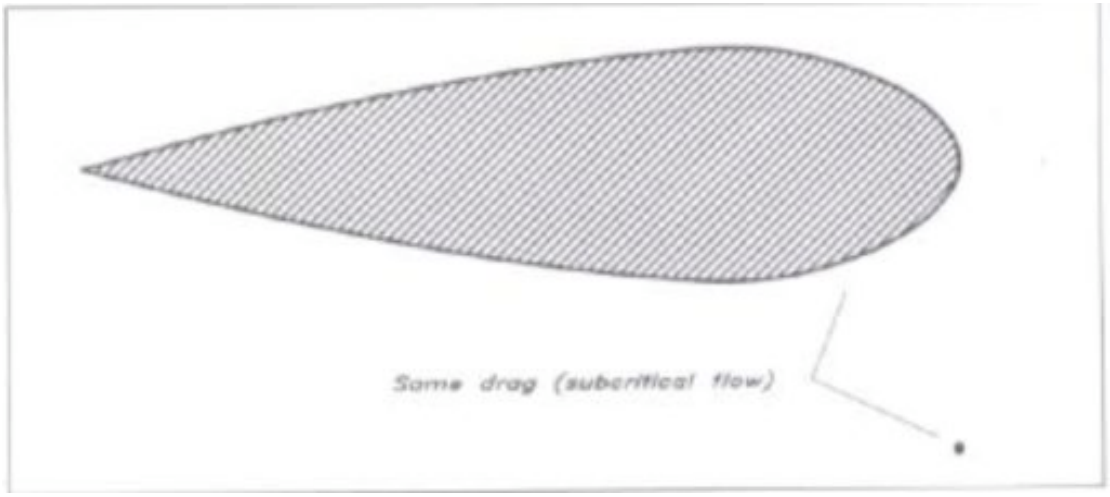

Figure 4-1 Equivalent drag force for optimized & circular bodies [13]

A priority is made to keep all equipment below deck and not to use stanchions to support the wing structure. The current anemometer support is not optimal due to financial restraints, however knowledge of the diameters of the wires and support pole diameter is enough to estimate the additional drag.

The two dominant forces on the hull are viscous and residuary (wave). The viscous friction component is estimated using the 1957 International Towing Tank Conference (ITTC) flat plate formula, the Delft Systematic Yacht Hull Series and wetted surface area calculations from the C.A.D model (Figure 2-5) [20].

$$C_f = \frac{0.075}{(Log_{10}\,\mathrm{Re} - 2)^2} \qquad \textbf{EQ 4-1}$$

$$F_f = \frac{1}{2} C_f \rho U^2 A_{Wetted}$$

Estimating the residuary resistance is more difficult, since its magnitude directly correlates to the geometry of the hull. With time it was decided that data from other hull shapes could be used as long as scaling factors were observed. The selected candidate is a YD-40, a forty foot hull with similar keel and rudder design to the 2.4 Meter (Figure 2-9). A substantial amount of test results are available, including a breakdown of all hull forces in Figure 4-2.

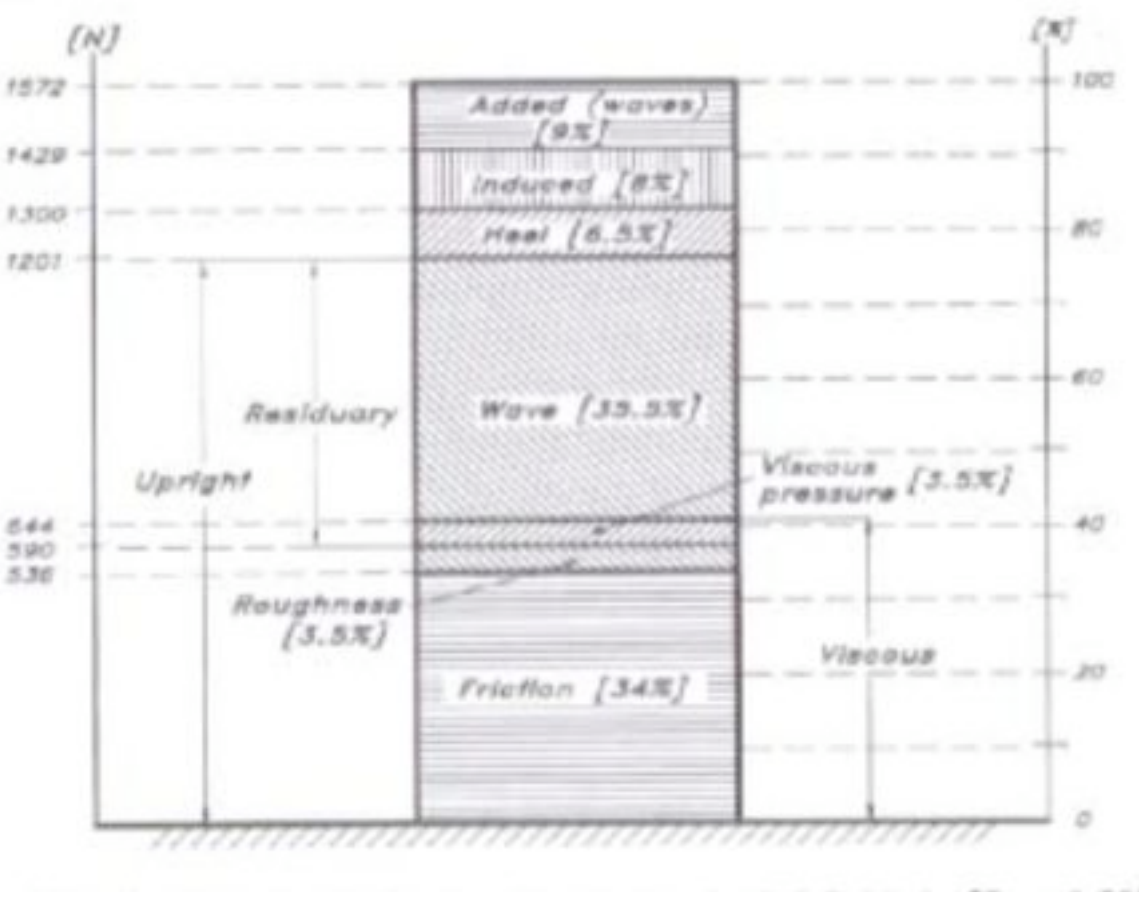

Figure 4-2 YD-40 Resistance Breakdown [15]

The resistances in Figure 4-2 represent a Froude number of 0.35, equivalent to a speed of 4.37 knots for the smaller 2.4 Meter hull (EQ 4-2).

$$F_n = 0.35 = \frac{U}{\sqrt{gL}}$$
$$U = 0.35 \times \sqrt{(9.81_{m/s^2})}(4.2_m) = 2.25_{m/s} = 4.37_{knots} \qquad \textbf{EQ 4-2}$$

Combining the relative percentages of Figure 4-2, the ITTC Formula in EQ 4-1, and the hull parameters from the C.A.D representation of the 2.4 Meter Hull, an initial estimation of the total resistance for different speeds can be determined. A roll criteria must also be considered, namely that the hull must maintain a roll angle of 45 degrees or less (the "stable point" from Figure 2-6). If this criteria is not met, the angle of attack of the wing must be reduced, effectively reducing the pressure gradient and overall force created by the wing. This is equivalent to "sheeting out" in nautical terms.

4.2 NUMERICAL MODEL CONDITIONS

(Balance) – The magnitude of the roll angle shall not exceed 45 degrees. If the roll angle does exceed 45 degrees, the angle of attack of the wing shall be reduced by one-degree increments until the condition is met.

$$\begin{aligned} &\textit{if} \quad && 2.83_m(F_{AS} + m_{wing}\sin(\frac{\pi}{4})) > D \cdot m_{keel}\sin(\frac{\pi}{4}) \\ &\textit{then} \quad && \alpha = \alpha_o - 1 \end{aligned}$$

(Tack Identification) – In order to trim the wing to the correct angle with respect to the wind, the control system will need to know what “tack” it is on. The numeric scheme is a function of the apparent wind angle.

$\beta = ApparentWindAngle = (heading - wind\ direction)$

if $\beta = 0$
then The WASP is pointing into the wind

if $|\beta| = 180$
then The WASP is pointing directly downwind

if $\beta > 180$
then The WASP is on Starboard Tack

if $0 < \beta < 180$
then The WASP is on Port Tack

if $\beta < -180$
then The WASP is on Port Tack

if $0 > \beta > -180$
then The WASP is on Starboard Tack

4.3 MATLAB SIMULATION

An iterative code in MATLAB is used to find the steady state equilibrium speed of the WASP in various wind conditions. The code can produce plots of speed, angle of attack, and equilibrium roll angle for all apparent wind angles.

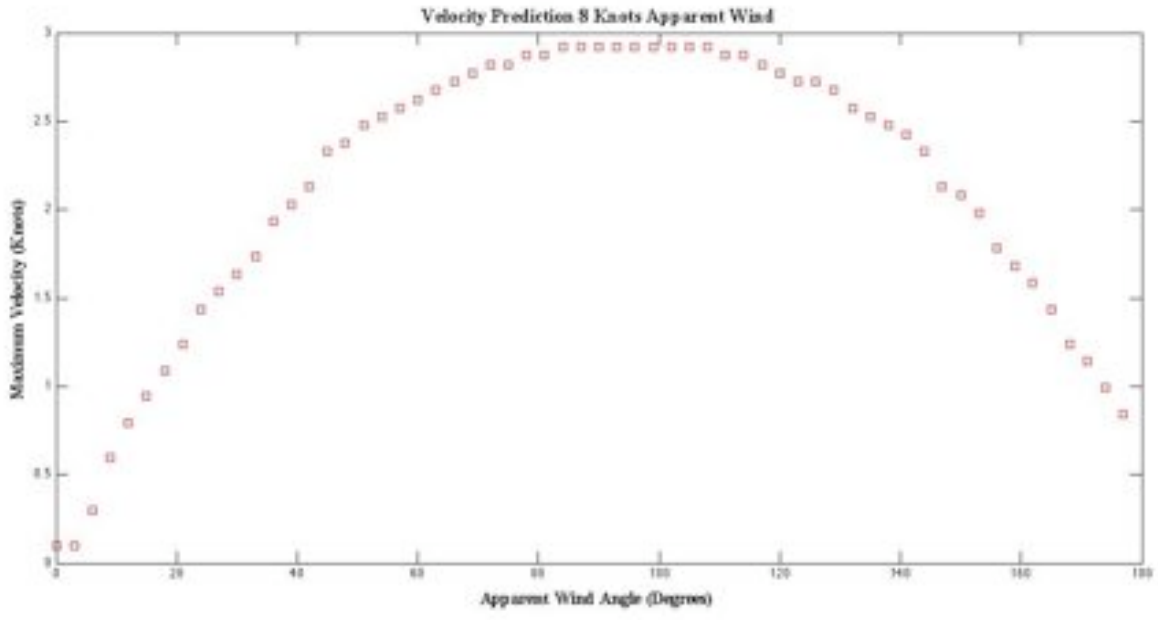

Figure 4-3 Initial Velocity Prediction 8 Knots

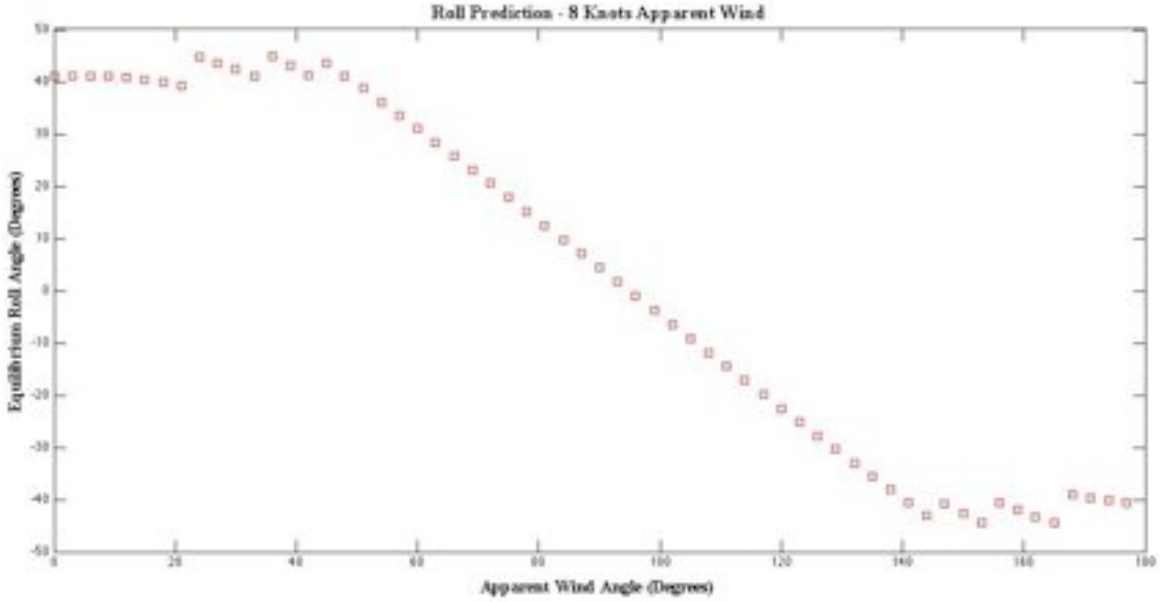

Figure 4-4 Initial Roll Angle Prediction 8 Knots

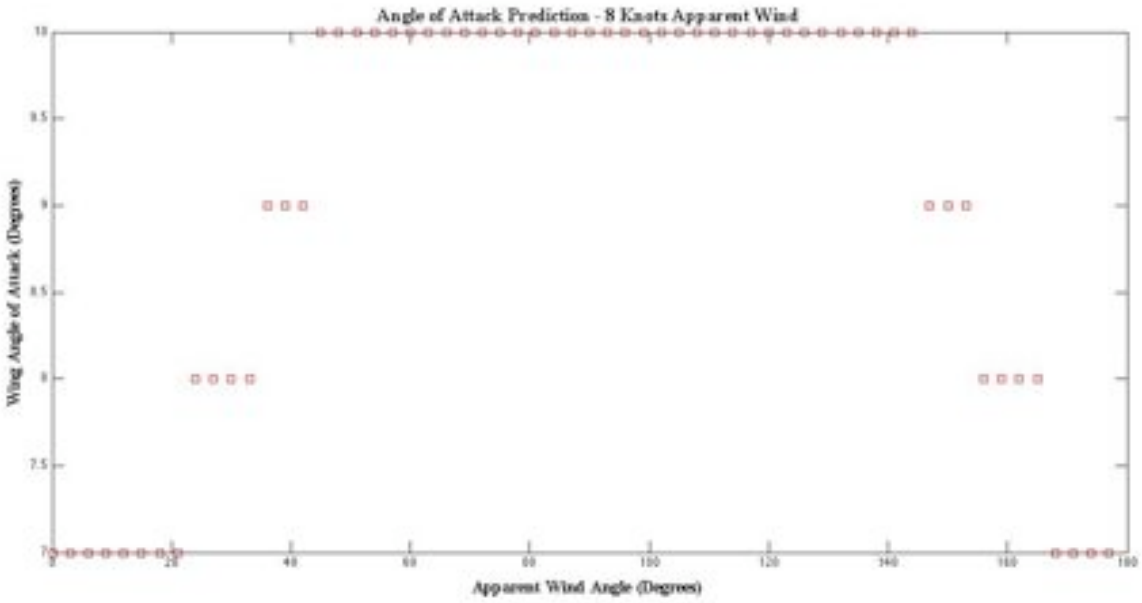

Figure 4-5 Initial Angle of Attack Prediction 8 Knots

The results of the first simulation are shown in Figure 4-3, 4-4, and 4-5. A notable feature is that the simulation succesfully recognized points when the wing angle of attack

must be reduced in order to maintain a roll angle less then 45 degrees. Some curious results are seen for apparent wind angles between 90 and 180 degrees. Typically sailboats exhibit positive roll angles (rolling in the direction the wind blows) and high speeds in this range. The simulation suggests negative roll angles (rolling in the direction the wind is blowing from) and slow speeds. Upon closer inspection, it became clear that the aerodynamics of a wing trimmed at a small angle of attack is substantially different then a classical cloth sail at these apparent wind angles. In a classical sailboat, the cloth sail performs like a lifting surface for apparent wind angles of less then around 90 degrees. For greater angles, however, the sail is trimmed such that it behaves like a parachute, or blunt body. Figure 4-6 illustrates the two modes. As a blunt body, the only force created is drag. Exactly where on the apparent wind curve is it beneficial to switch modes, or more accurately, when does the aerodynamic driving force of the blunt body wing equal that of the lifting surface?

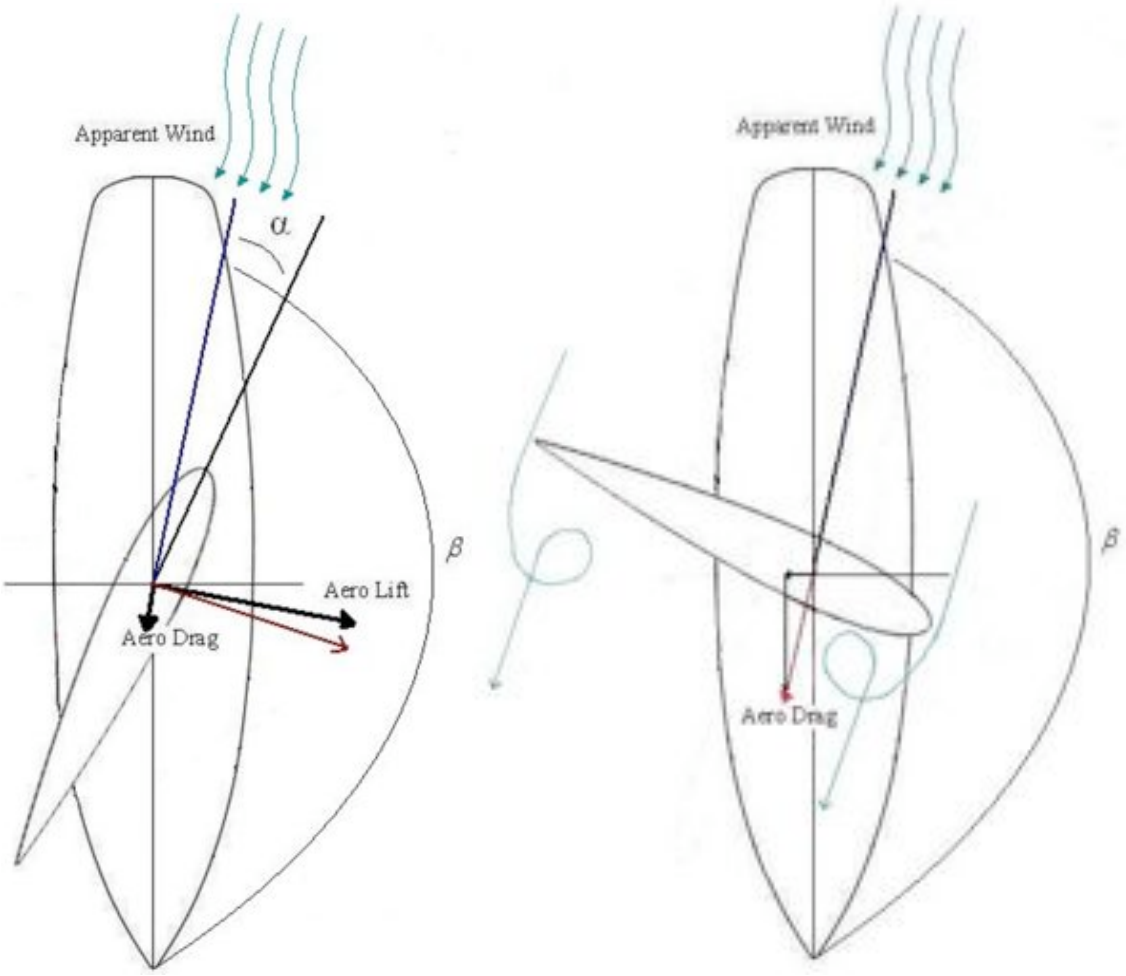

Figure 4-6 Downwind Trimming Criteria's

Wing vs. Blunt Body

Wing

$C_L \approx 1.0506 \qquad C_D \approx 0.091$

Rectangular *Blunt Body*

$C_L \approx 0 \qquad C_D \approx 1.2$

EQ 4-3

$$F_{ARWING} = \sin(\beta - \tan^{-1}(\frac{C_D}{C_L}))\sqrt{(\frac{1}{4}\rho^2 U^4 A^2)({C_L}^2 + {C_D}^2)}$$

$$F_{ARBLUNT} = \sin(\beta - \tan^{-1}(\frac{C_D}{0}))\sqrt{(\frac{1}{4}\rho^2 U^4 A^2)({C_D}^2)}$$

$$\sin(\beta - \tan^{-1}(\frac{C_D}{C_L}))\sqrt{(\frac{1}{4}\rho^2 U^4 A^2)({C_L}^2 + {C_D}^2)} = \sin(\beta - \tan^{-1}(\frac{C_D}{0}))\sqrt{(\frac{1}{4}\rho^2 U^4 A^2)({C_D}^2)}$$

$$\frac{\sin(\beta - \tan^{-1}(\frac{C_D}{C_L}))}{\sin(\beta - \tan^{-1}(\frac{C_D}{0}))} = \frac{\sqrt{(\frac{1}{4}\rho^2 U^4 A^2)({C_D}^2)}}{\sqrt{(\frac{1}{4}\rho^2 U^4 A^2)({C_L}^2 + {C_D}^2)}} = \sqrt{\frac{(1.2^2)}{(1.0506^2 + 0.091^2)}}$$

$$\frac{\sin(\beta - 4.95^\circ)}{\sin(\beta - 90^\circ)} = 1.295$$

$$\beta = 135^\circ - 4.95^\circ = 135^\circ - \tan^{-1}(\frac{C_D}{C_L}) = 130.05^\circ$$

This result of EQ 4-3 suggests that it is more beneficial to turn the wing 90 degrees to the apparent wind when the apparent wind angle is greater then approximately 130 degrees. Running the simulation with this criteria produces Figure 4-7, 4-8, and 4-9.

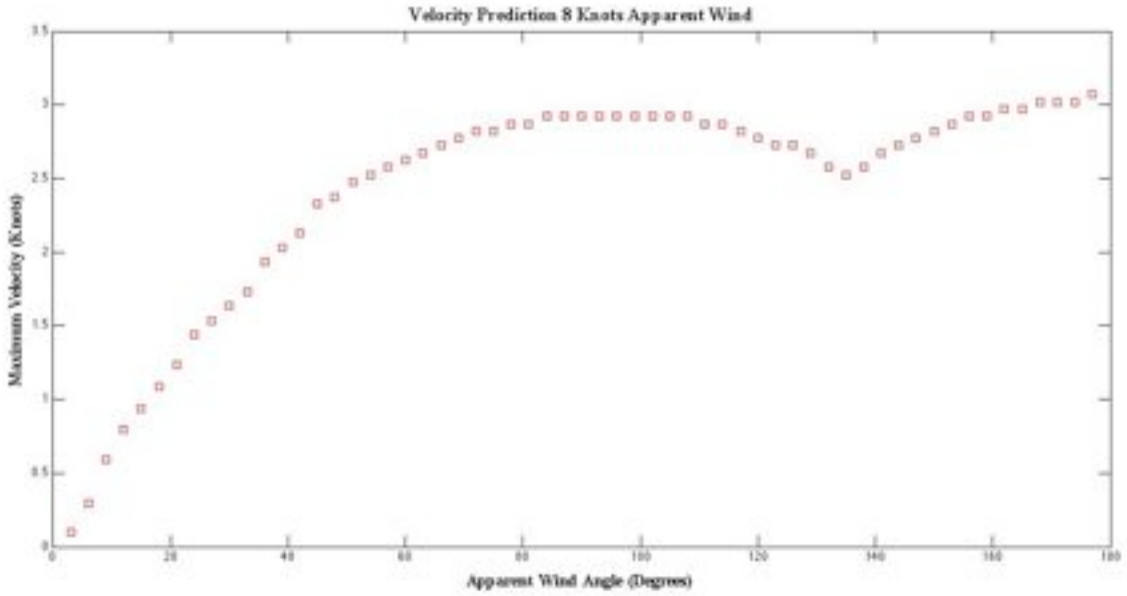

Figure 4-7 Final Velocity Prediction 8 Knots

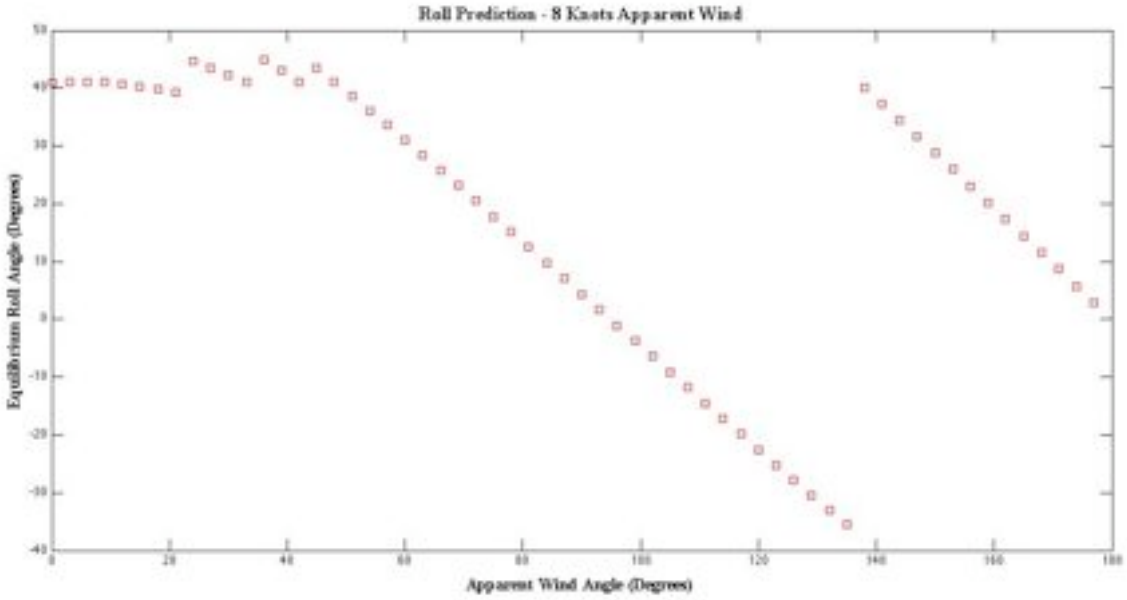

Figure 4-8 Final Roll Prediction 8 Knots

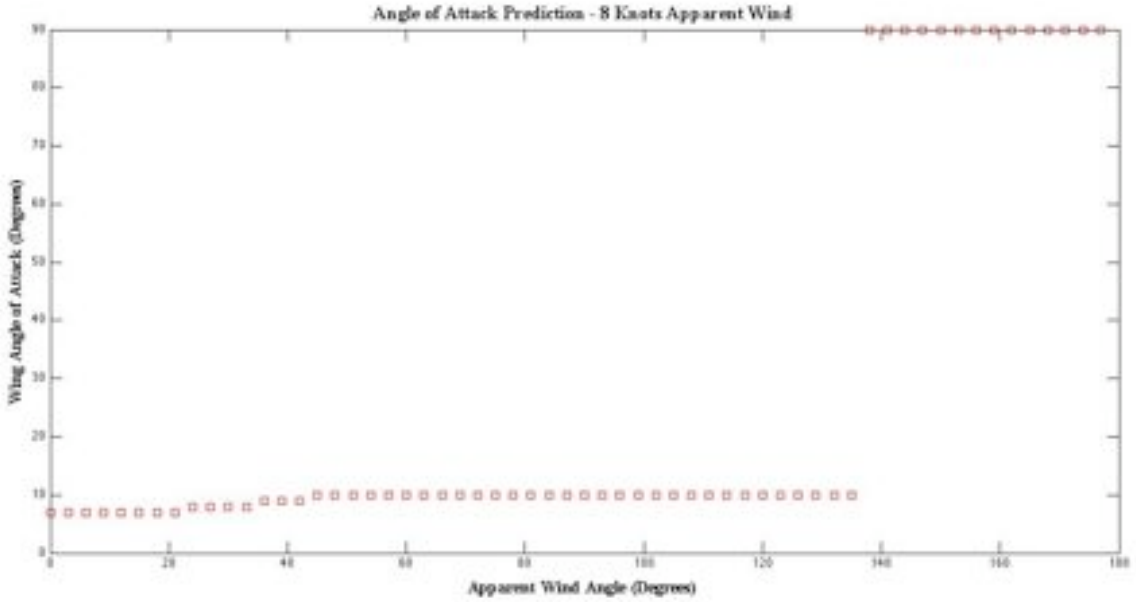

Figure 4-9 Final Angle of Attack Prediction 8 Knots

The velocity prediction for apparent wind angles greater then 90 degrees reflect known qualities of sailboats, namely that "downwind" speed peaks at 90 degrees and 180 degrees to the wind for displacement hull designs (hulls that do not plane). Figure 4-7 suggests that the roll angle will be negative for angles greater then 90 degrees and less then approximately 135 degrees. This is an interesting result, and attention will be placed on this apparent wind angle range during sea trials.

4.4 AUTONOMOUS CONTROL

The control system was treated as a combination of de-coupled subsystems; rudder control and sail control. The trimming scheme developed from the numeric model presented in Section 4-2 was used in the development of a control algorithm. FAU M.S graduate student Michael Tall wrote the code for the algorithm in the C/C++ programming language. Specific details of the system, including hardware identification

and calibration processes are presented in the Florida Atlantic University 2007-2008 Senior Design Course Final Report. [19]

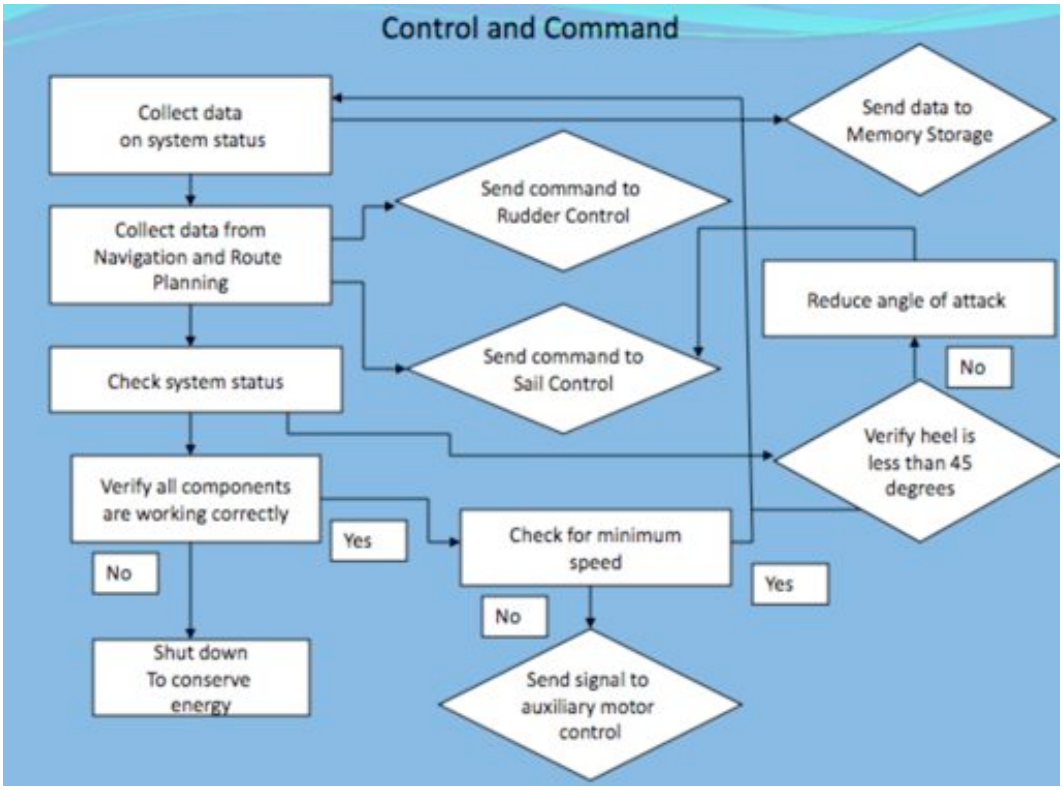

Figure 4-10 Command & Control Structure [19]

A command and control scheme is presented in Figure 4-10 and a hardware diagram in Figure 4-11. The initial control system operates a basic proportional controller for the rudder and a scalar "trimming code" for the wing. During the testing outlined in Section 6, the rudder was controlled by a human via Bluetooth Modem due to security issues with the testing area and time constraints.

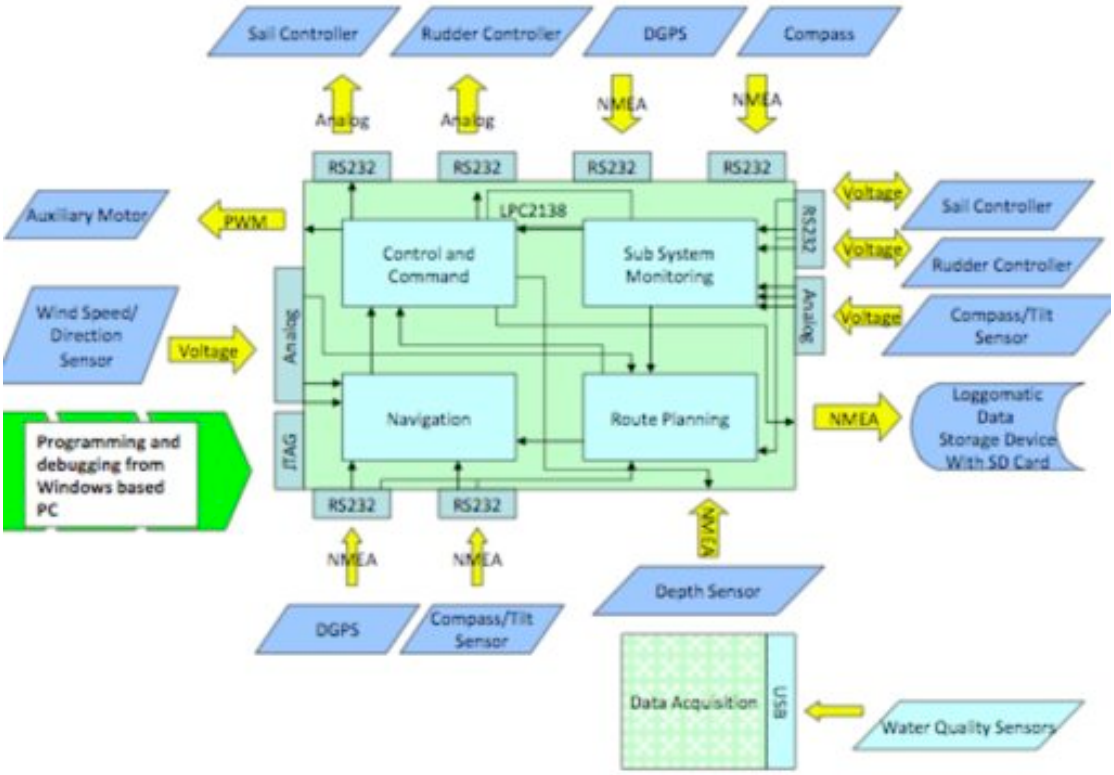

Figure 4-11 Functional block diagram of command & control system [19]

5 Results

Four sea trials were conducted during September and October 2008. Two of the missions were conducted under wind power while the rest were propeller driven. The goal of the experiments was to attain oceanographic data while developing the control and data acquisition system. An outline of the navigation and oceanographic sensors is presented in Figure 5-1.

Navigation & Control	Global Position	32 Channel Etek GPS
	Heading	OS5000-S Tilt Compensated Compass
	Wind Speed & Direction	200-WS-02 NovaLynx Anemometer
	Processing	LPC-2138 ARM Microcontroller
Oceanographic	Water Temperature	Vernier Go Temp Sensor
	Oxidation Reduction Potential	Vernier Redox Potential Sensor
	Salinity	Vernier Salinity Sensor

Figure 5-1 Sensors Overview

The Intracoastal Waterway immediately north of the FAU Seatech campus extending approximately 2 miles farther north into Port Everglades was selected as the testing area. Specific focus was placed on tracking water quality around the Dania Cutoff Canal (a brackish water channel) and the outflow from a nearby power plant, which creates a thermal plume. For these missions, the rudder angle of the vehicle was manually controlled due to the proximity of the testing sites to high security areas.

5.1 SEA TRIAL - 09/12/08

The first experiment was conducted within the Sea Tech marina in an oscillating 5-knot easterly wind. There were no waves in the testing area and the tide was slack (no visible current). The experiment lasted 10 minutes. After completion of the experiment it became clear that no oceanographic data had been collected due to a software error. The rudder angle was controlled from shore using a Bluetooth modem.

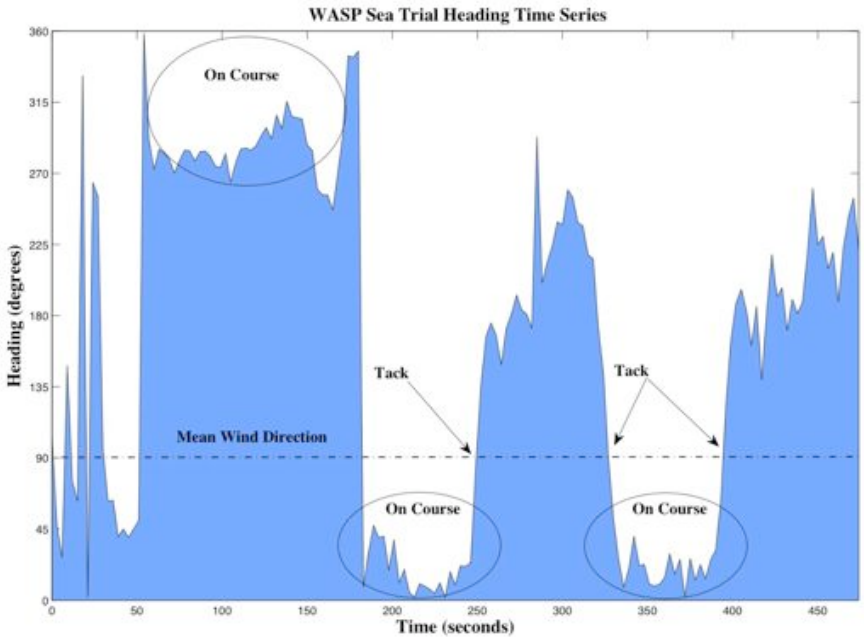

Figure 5-2 09/12/08 Sea Trial Heading Time Series

The heading of the WASP during the manuevers is presented in Figure 5-2. The highlighted regions illustrate a straight course and turning manuever. Although minimum rudder changes were made during the straight segments of the test, the change in wind strength and direction affected the roll angle significantly. The varying roll angle induced yawing moments as shown in Figure 2-7 and account for the oscillations in the heading.

The WASP speed over ground and windspeed time series are shown in Figures 5-3 and 5-4. Although this data does not represent a constant

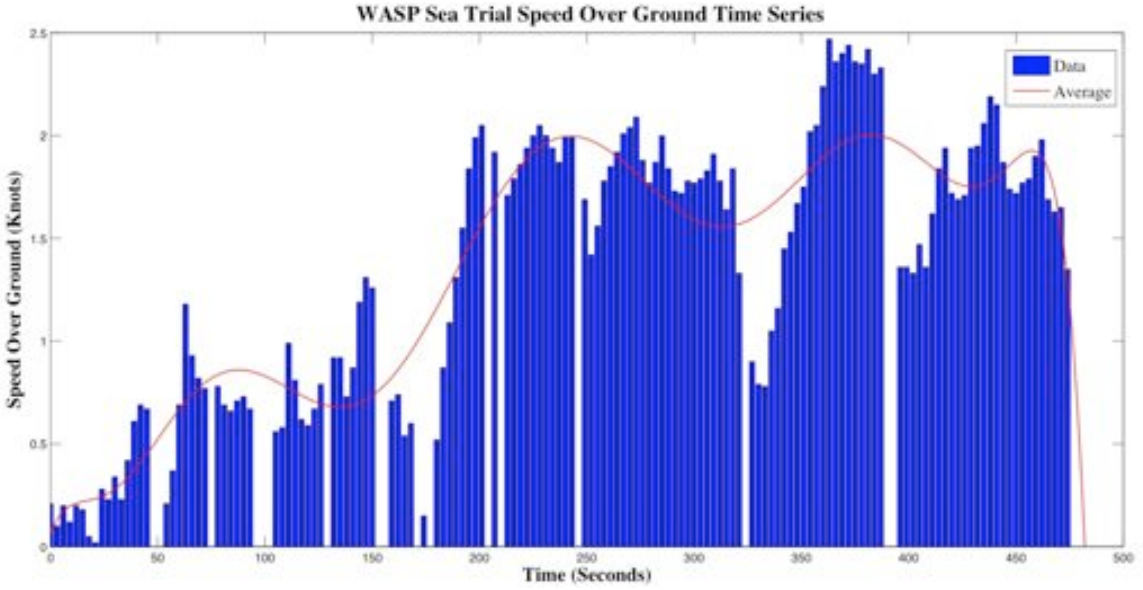

Figure 5-3 09/12/08 Sea Trial Speed Over Ground Time Series

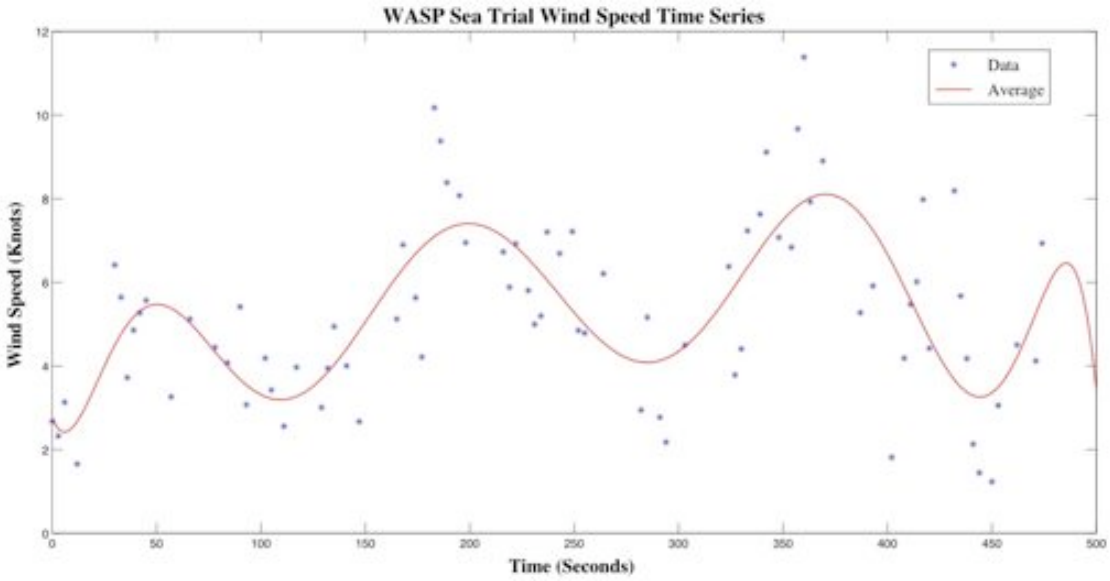

Figure 5-4 09/12/08 Sea Trial Wind speed Time Series

heading, there appears to be a correlation between the two data sets. The cross-correlation coefficient values between speed over ground and wind speed, however were surprisingly small (not shown). This is likely caused by the turning maneuvers that occurred during the data collection. Therefore, along with collecting oceanographic data, the second experiment focuses on recording speed over ground and wind speed over a long distance without turning for cross-correlation analysis.

Due to the lack of surface waves during the experiment, this data was used to analyze the accuracy of the velocity prediction program outlined in Chapter 5. Figure 5-5 suggests that the VPP provides a suprisingly accurate represenation for flat water conditions. Some data processing was implemented in this figure, namely that the data correlating with a turning manuever were removed. These data points suggested high speeds at low apparent wind angles, but were logically a result of momentum rather then steady state equilibrium.

5.2 SEA TRIAL – 10/06/08

A second experiment was performed in hopes of acquiring oceanographic measurements and straight-line performance data for correlation analysis. The testing area was a one-mile section of the Intracoastal Waterway immediately north of the Seatech Campus (Figure 5-6). The wind strength was substantially greater then it was in the previous experiment, with gusts approaching 20 knots. Rudder angle was controlled with a Bluetooth modem and a human subject sat aboard for emergency purposes. The WASP performed well on straight sections, but suffered from instability during tacking and jibing maneuvers. The main problem appeared to be momentum induced rolling caused by oscillating wind during a tacking maneuver. When executing a tack, the bow of the boat turns through the wind and the angle of attack shifts accordingly. When the wing is crossing through a zero angle of attack position, it is capable of creating lift on either tack in response to a small wind direction shift. Equation 2-3 suggests that the aerodynamic side force reaches a peak value as the apparent wind angle approaches zero. This is a bad situation in strong, oscillating winds, and was realized in the form of a "double capsize" during this mission. Due to the capsize and a leak in the deck cover, the oceanographic data acquisition computer was destroyed and the data was lost.

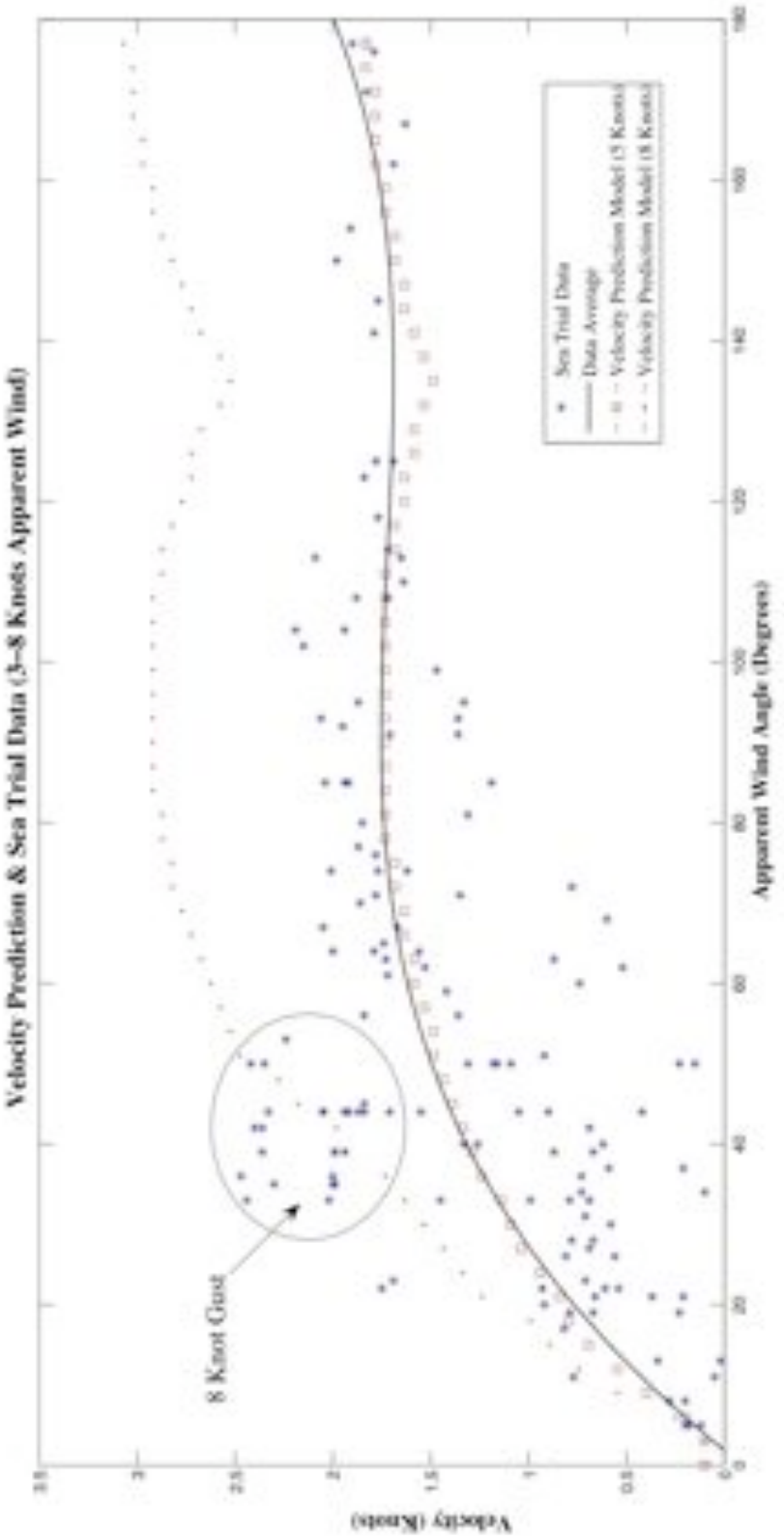

Figure 5-5 09/12/08 Sea Trial S.O.G Distribution

Figure 5-6 10/06/08 Sea Trial GPS Plot (Sailing) [20]

Figure 5-7 10/06/08 Sea Trial S.O.G Time Series

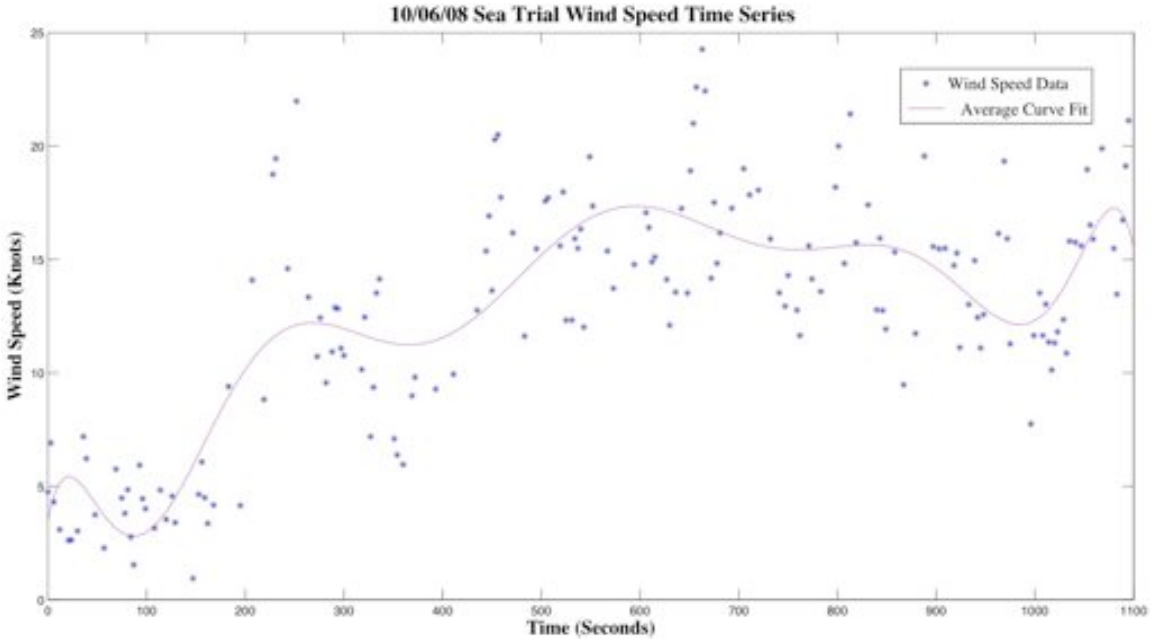

Figure 5-8 10/06/08 Sea Trial Wind Speed Time Series

A 20-minute segment of the mission is presented in Figures 5-7 and 5-8. As in Figures 5-3 and 5-4, there appears to be a correlation between the data. Because this

mission was a straight run without major turns (except for the one turn encircled in Figure 5-7), cross-correlation analysis between wind speeds and speed over ground should be more accurate then the previous experiment. Specific attention is given to the period of acceleration during the first 400 seconds of the run. Figure 5-9 provides a zoomed in view of normalized speed over ground and wind speed. Both data sets are normalized with their respective mean values. Projecting both series onto one plot suggests a near zero lag between the two variables. Cross-Correlation between speed over ground and wind speed is presented in Figure 5-10. The high cross-correlation coefficient also suggests that the data is highly correlated at zero lag.

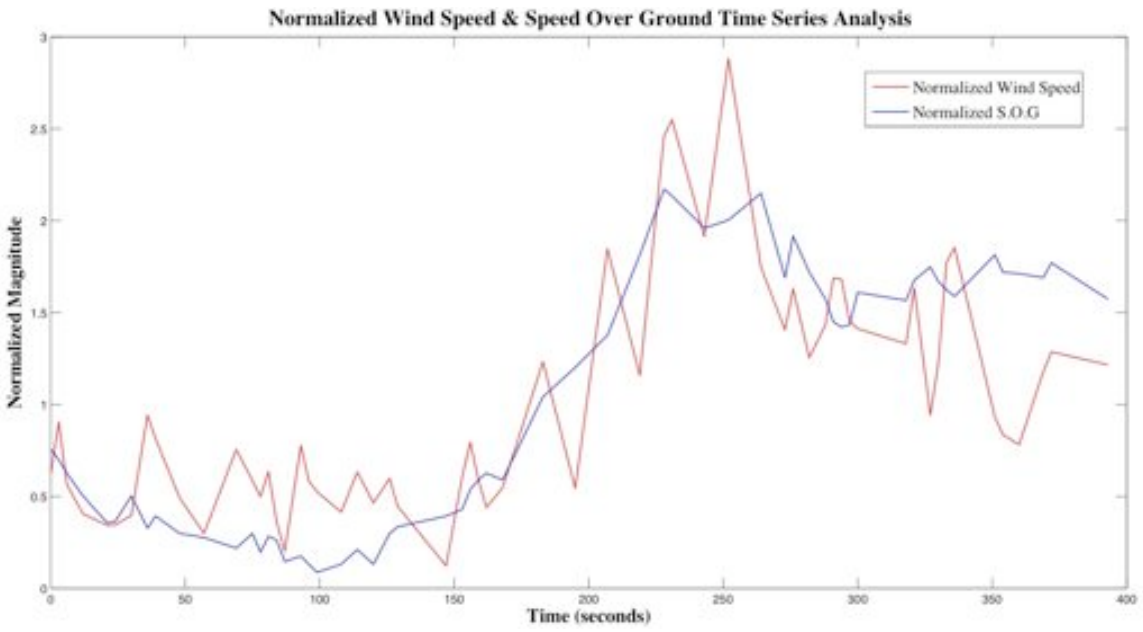

Figure 5-9 10/06/08 Zoomed-In Normalized Time Series

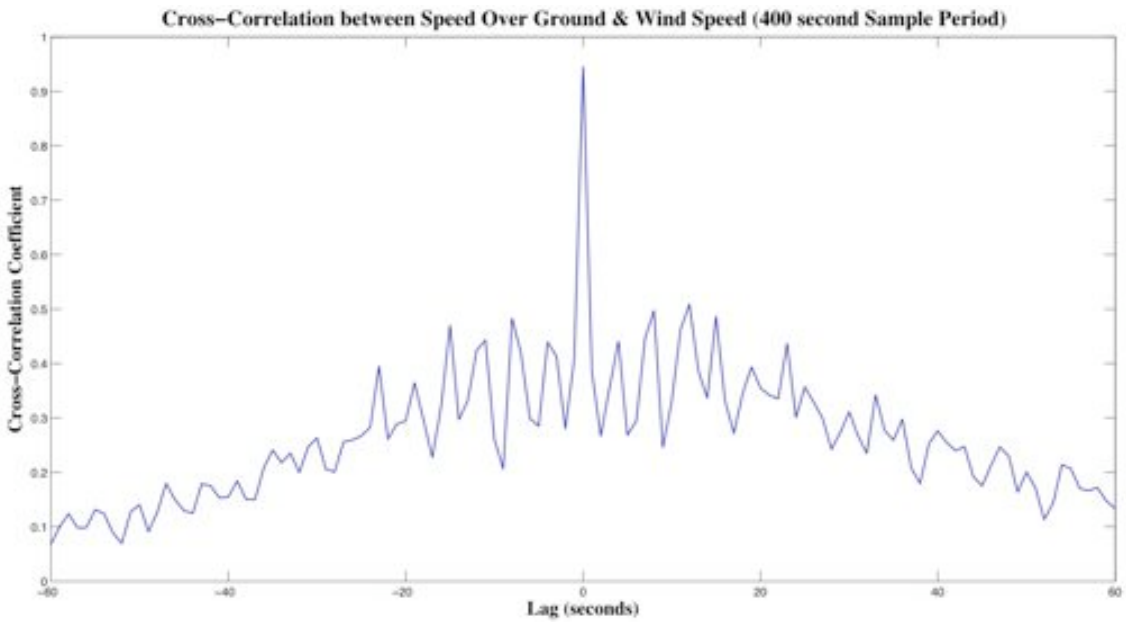

Figure 5-10 10/06/08 Zoomed-In Cross Correlation between S.O.G & wind speed

It was expected that there would be a non-zero lag for the maximum correlation between wind speed and boat speed. The easiest way to think of this is to consider how the WASP would respond to an instantanous increase in wind from a zero wind initial condition. Newton's second law implies that the boat will accelerate over time and eventually reach a steady state equilibrium speed in ideal conditions. The delay between when the wind is applied and when the WASP reaches steady state is the lag time expected in a cross-correlation analysis. One possible source of problem is that the wind speed recorded is the apparent wind, not the true wind. Similar to holding your hand out the window of a moving car and feeling wind, what the on-board anemometer senses does not represent the true wind strength. Knowing the heading, speed over ground, apparent wind direction and magnitude is enough to determine an estimate of the true wind in EQ 5-1.

$\beta = Apparent\ Wind\ Angle$

$W = Apparent\ Wind\ Magnitude$

$SOG = WASP\ Speed\ Over\ Ground$

$$True\ Wind\ Magnitude = \sqrt{\{(W\cos(90-\beta))^2 + (W\sin(90-\beta) - SOG)^2\}}$$

$$True\ Wind\ Angle = 90 - \tan^{-1}\left(\frac{W\sin(90-\beta) - SOG}{W\cos(90-\beta)}\right)$$

EQ 5-1

A 400 second sample of the true wind strength is shown in Figure 5-11. During this period, the WASP was maintaining a course with an average apparent wind angle of approximately 45 degrees. When the apparent wind angle is less then 90 degrees, the apparent change in wind strength is positive (the WASP "feels" like it is windier then it really is). Conversely, when the apparent wind angle is greater then ninety degrees, the apparent change in wind strength is negative. Cross-Correlation between true wind and speed over ground is presented in Figure 5-12, and projected against the apparent wind cross-correlation. The effect of the apparent wind shift on the lag period appears to be negligible.

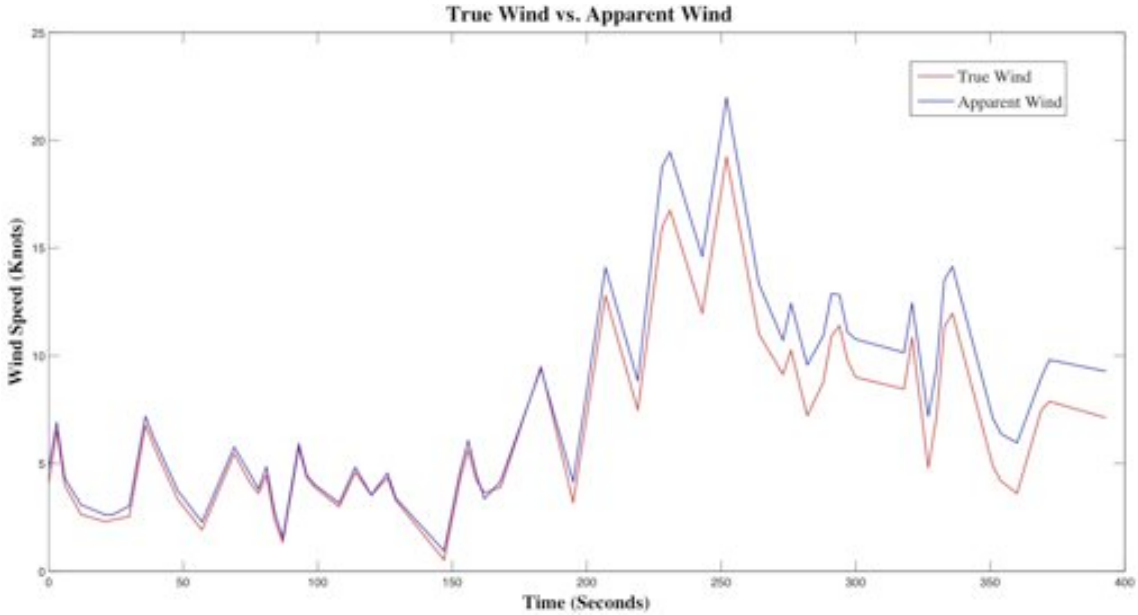

Figure 5-11 10/06/08 Apparent Wind vs. True Wind

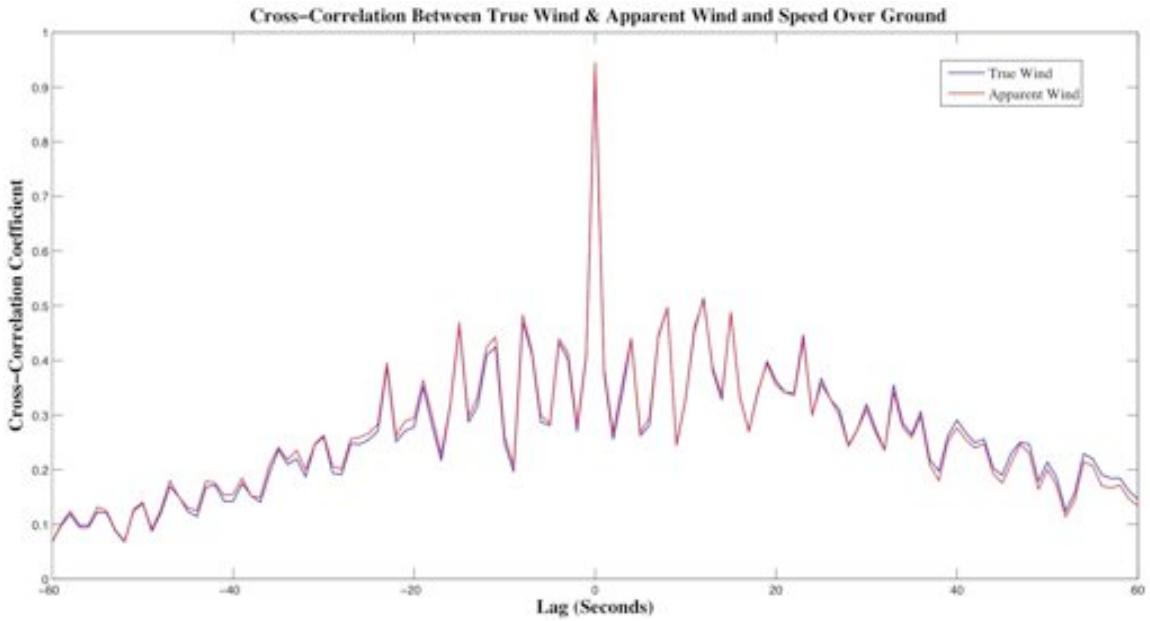

Figure 5-12 10/06/08 True Wind Cross-Correlation Comparison

The effect of current is another significant factor in analyzing the speed over ground data. Although the testing was conducted during slack tide, there was significant visible current. At the beginning of the experiment the WASP was tethered to a chase boat and held stationary. The two craft drifted with the current and the data was used to estimate the current strength for post-processing of the speed over ground values. Unfortunately, the current at the beginning of the experiment was significantly less then farther downstream. Figure 5-13 is an unprocessed distribution of speed over ground versus apparent wind angle. Because the wind strength was reasonably steady throughout the mission(12.58 knots average, 5 knot standard deviation), the "ladder rung" nature of the distribution suggests that there were regions of different current strength. This is not surprising since the experiment was conducted in regions of both weak and very strong current.

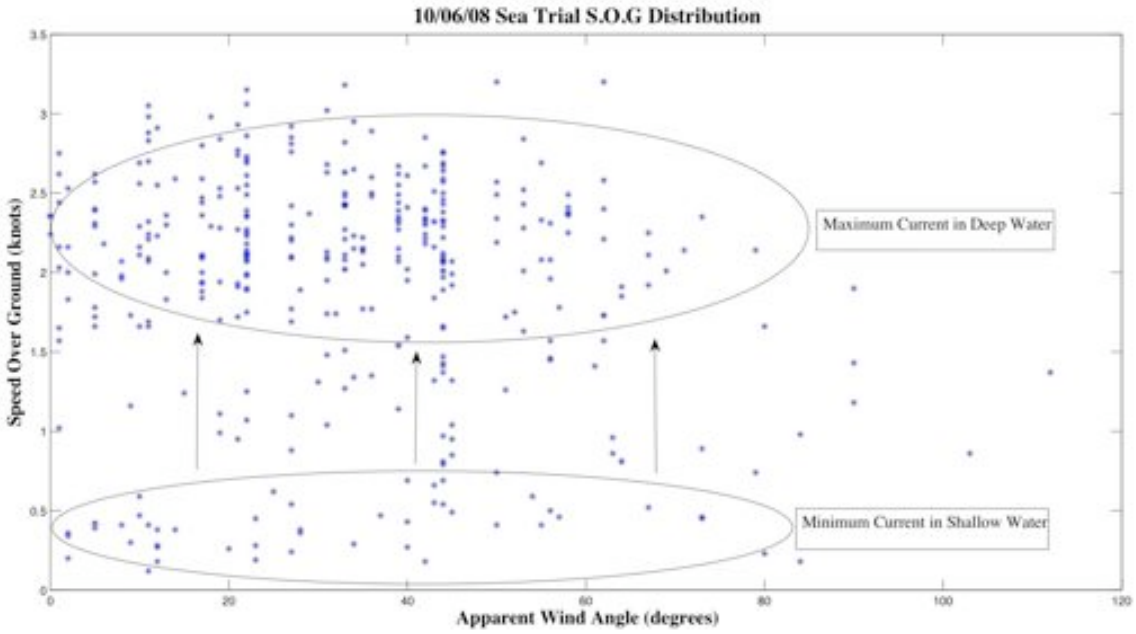

Figure 5-13 10/06/08 S.O.G Distribution

5.3 SEA TRIAL – 10/12/08

A third sea trial failed to acquire substantial oceanographic data due to sensor calibration problems. A successful fourth and final experiment was performed using auxiliary propulsion (propeller) due to a lack of wind. The experiment was conducted during a strong incoming tide.

Figure 5-14 10/12/08 Sea Trial GPS Plot [20]

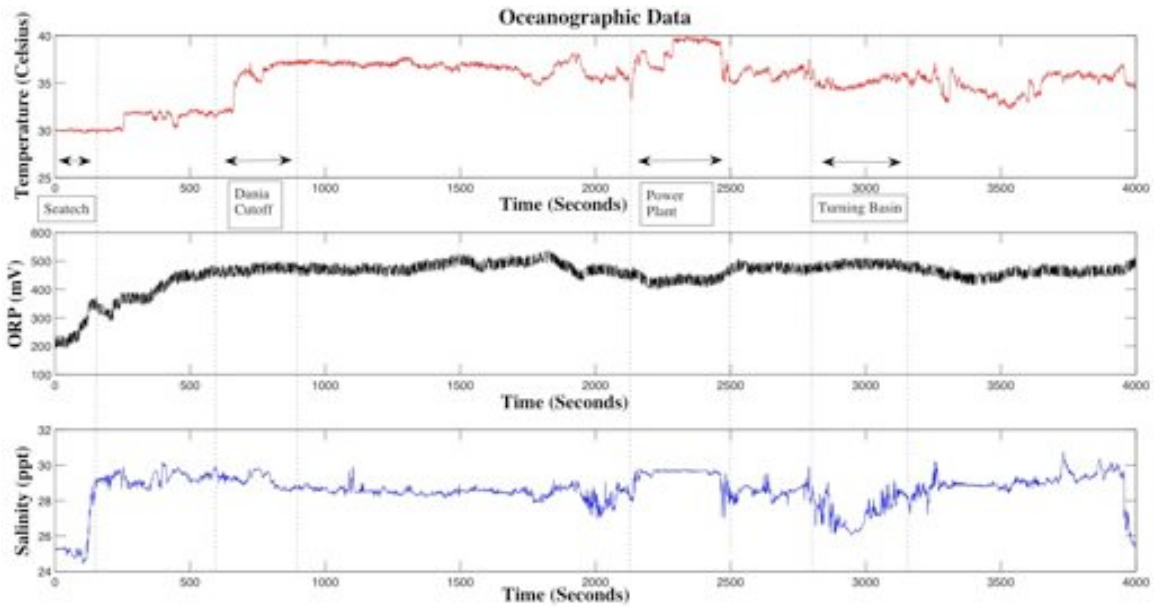

Figure 5-15 10/12/08 Oceanographic Observations

A course map is presented in Figure 5-14 and over one hour of observations are presented in Figure 5-15. Because the oceanographic data acquisition system is entirely separate from the navigation system, both respective time stamp functions were initiated at the same time in order to match GPS data with water measurements. Mission time was also recorded on a stopwatch and human observations were written down during the experiment. The time stamps from the GPS were matched with the oceanographic data and also with the stopwatch and human observations. Having two levels of redundancy is important in insuring that the oceanographic data accurately represents specific GPS positions. Three distinct features of interest are highlighted in Figure 5-15. The first is the change in water properties when exiting the Seatech marina and entering the strong flow of the Intracoastal Waterway (Figure 5-16).

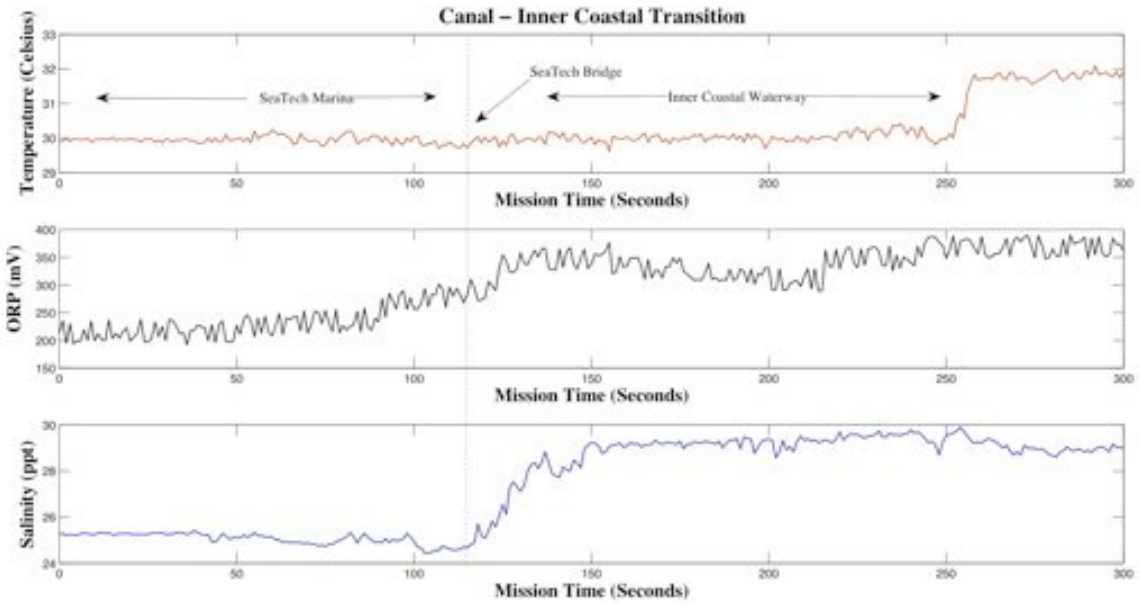

Figure 5-16 10/12/08 Canal Transition to Intracoastal Waterway

Salinity values around 25 ppt suggest that the water around the Seatech marina is brackish. Salinity is a measurement of dissolved salt content, with Atlantic Ocean surface averages between 33 and 37 parts per thousand [21]. The Seatech marina is located at the entrance of an estuary that extends approximately two miles north. These areas are known to create brackish water due to their isolation from the primary flow from the ocean. The salinity jumped significantly upon crossing under the Seatech bridge into the intracoastal waterway. This spike in salinity could represent the location of a circulation feature caused by the geometry of the estuary inlet and the strong current within the waterway.

Oxidation reduction potential is a measurement of the ability of a substance to oxidize another material. Strong oxidizing agents such as Chlorine make good purifiers due to their affinity for electrons, a property that facilitates the breakdown of impurities. In general terms, high ORP measurements represent samples with strong oxidation

potential, or an excess of oxidizing agents compared to impurities. The ORP values within Seatech were the lowest of the series, suggesting the body of water has the least oxidizing potential and is likely to be the dirtiest [22]. It is important to note that the ORP scale is relative to the sensor used. Our sensor was calibrated in dionized water with ORP levels around 200 mV. Like the salinity, the ORP values increased significantly upon crossing into the intracoastal waterway. It is important to recall that the experiment was conducted during an incoming tide. It is expected that the water flooding into the waterway from the ocean would be "cleaner" then the stagnant estuaries. It is recomended that the recorded values be compared to those during an outgoing tide to determine if ebbing estuaries correlate to decreased ORP readings within the waterway.

Water temperature is the most important measurement of the experiment due to its ability to clearly mark the region affected by the power plant cooling station. The first notable feature of the temperature series is the lag between the salinity and ORP spikes at 120 seconds in Figure 5-16 yet the first temperature spike occurs at 250 seconds. Referring to our mission log book, the WASP ran aground shortly after exiting the estuary at 157 seconds, became free at 208 seconds, and entered the intracoastal at 248 seconds. The temperature spike therefore is attributed to entering the strong incoming flow of the flooding tide following the delay caused by running aground.

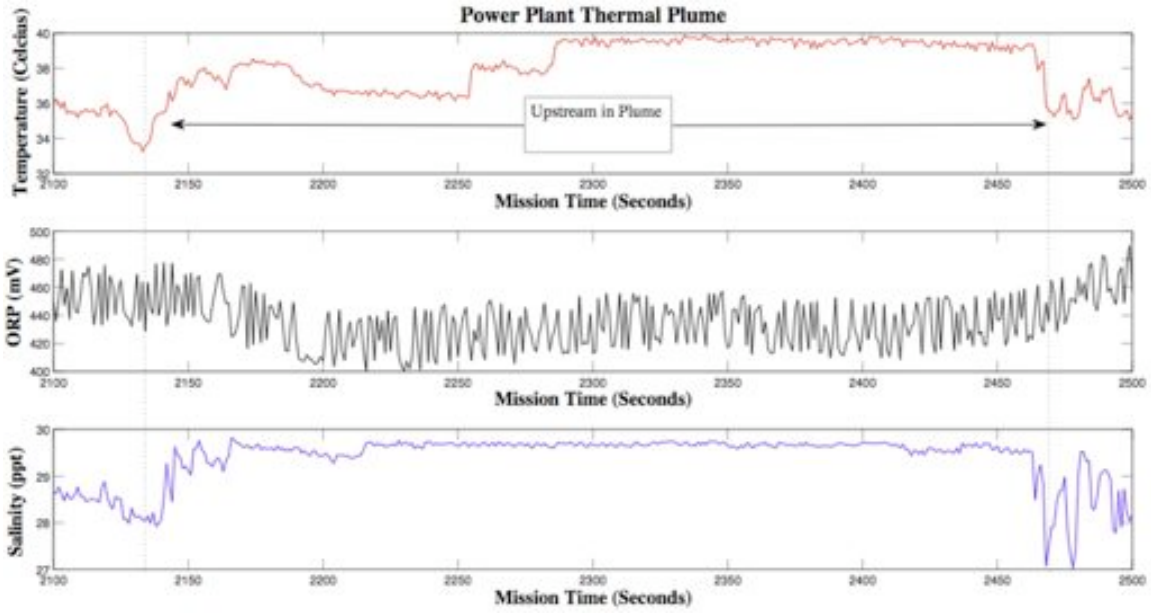

Figure 5-17 10/12/08 Thermal Plume

The second feature of interest is highlighted in Figure 5-17 and represents data acquired at the entrance of a power plant outflow inlet immediately south of Port Everglades. The prominent feature of the samples is a very high water temperature. Temperatures upstream in the inlet nearly reach 40 degree Celsius (104 degrees Fahrenheit). Due to the magnitude of this outflow temperature and the northerly current (incoming tide), it is likely that the elevated readings found far downstream in Figure 5-15 are caused by the power plant.

Figure 5-17 also shows a small drop in ORP and rise in salinity within the outflow inlet. The reduction in ORP could represent an increase of impurites coming from the power plant cooling station. Future work with different ORP sensors including a control environment analysis would be needed to justify this claim. The salinity readings in this region were the highest of the series and very stable. It is well known that the solubility

of salt in water increases with increasing temperature, which could cause the elevated readings.

6 Conclusions & Future Recommendations

The combination of a light weight composite wing sail with the self-righting ability of a mono hull provides the performance and stability that is needed in an open ocean environment.

6.1 CONCLUSIONS

The Hull – One oversight regarding the 2.4 Meter Sailboat was our inability to fit enough lead counterweight in the keel. The volume of the keel trunk was estimated by measuring the area of the cross section and multiplying it by the draft. The volume was multiplied by the density of lead to determine the maximum counterweight available. The mistake was that lead shot in individual bags is less dense then solid lead, leading to a reduction in counterweight by approximately 30%. If the 2.4 Meter Sailboat design were

to be utilized for future efforts, it would be beneficial to add a bulb keel or to increase the draft of the existing keel. It was also concluded that the size of the rudder was too small for a reliable system. Because of its small size, the rudder was unable to counteract the yawing moment induced by large angles of roll. An increased area, high-aspect ratio rudder would make a better choice for future efforts.

The Wing – Decreasing the weight of the wing without sacrificing its structural integrity would increase the overall performance of the system. With the experience of building one wing, designing future versions will be far easier. The weight of the wing, however could still be reduced. The main weight contributor was the leading edge shell which consisted of 5 layers of featherweight cloth. In retrospect, I estimate that three layers would have been sufficiently strong.

The scaling of the wing should also be reconsidered in future efforts. The wing was scaled to provide the same power as the existing sail plan. It was the opinion of trained 2.4 Meter Class sailors that the existing sail plan was "overpowering" in moderate winds. This held true with the wing. A WASP with a smaller wing would go slower, but would have a higher wind range then too large of a wing. It would be better to be slow in light wind than capsized in heavy.

The System – The WASP system would benefit from being less cumbersome. One of the main goals with any research instrument is to facilitate simple deployment and recovery schemes. Employing a deeper draft bulb keel and a lighter wing would address this issue.

6.2 FUTURE WORK

Due to substantial interest in the ocean science and engineering community in acquiring both long-term and long-range ocean observations, the pursuit of future versions of the WASP is justified. Future designs must be tailored to their specific mission, but both larger and smaller versions could address various research tasks within the community.

A significant challenge for the future development of unmanned wind-powered autonomous surface vehicles is the modification of the legal framework that defines the "rules" for ocean vehicles. An unmanned autonomous surface vehicle is not directly identified by the "International Regulations for Prevention of Collision at Sea", or "COLREGS" (United States Coast Guard, 1972). Benjamin *et al* [25] use behavior-based control and an interval-programming model to control two autonomous kayaks within the constraints of the COLREGS rules. Other unmanned autonomous surface vehicles have been designed to use mast mounted day shapes and lights to alert other vessels that the vehicle is Not Under Command (NUC) as prescribed by COLREGS Rule 27 [26]. These recent works represent the effort of the scientific community to abide by the current laws

as best as possible. It appears, however, that maritime laws including the COLREGS rules and Longshore and Harbor Workers Compensation Act (LHWCA) must be re-examined [27] with respect to vehicle classification.

7 Appendix

7.1 WING FABRICATION

The wing was constructed in three processes; foam cutting, fiberglass reinforcement, and assembly. Each rib was cut from a section of syntactic foam using a CNC machine. The ribs were reinforced with fiberglass and epoxy resin using a pressure technique without the use of a vacuum bag. After applying the cloth and saturating it with resin, electrical tape was wrapped around the entire section, and pulled tight to squeeze out excess resin (Figure 7-1). The result is a nearly uniform resin level, and a high strength to weight ratio. Upon curing, each rib was sanded until all excess resin was removed and weighed on a scale to confirm weight consistency.

Figure 7-1 Electrical Tape Pressure Method

Fabricating a leading edge shell requires a mold with which to shape the fiberglass cloth. The process is two-fold. First a male plug is cut from high-density syntactic foam using a CNC machine (Figure 7-2) using IGES files from Pro-Engineer. Because the mold must be five meters long, and the CNC machine can only cut one-meter increments, the mold was assembled in sections (Figure 7-3, Figure 7-4).

Figure 7-2 Jason Engle fabricating a plug section

Figure 7-3 Plug Sections ready for alignment

Figure 7-4 Aligned plug sections after sanding

The mold was then covered with a layer of gel coat and sprayed with a water-based mold release agent, followed by another layer of gel coat. A thin layer of three-ounce fiberglass was then carefully applied first with a polyester thermosetting resin (Figure 7-5). Polyester resin was used for construction of the mold to reduce cost, but required more extensive safety equipment. Five more layers of thick fiberglass were added to provide structural support for the mold. The mold was left to cure for a week, and then released from the plug easily (Figure 7-6). The surface of the mold was polished, and more layers of mold release were applied, followed by another layer of gel coat. These layers of gel coat would be the exterior finish of the final leading edge shell. Seven thin layers of fiberglass, four layers of three-ounce cloth and three of

Figure 7-5 Applying fiberglass and resin to plug

Figure 7-6 Final female mold

featherweight “veil” cloths were carefully applied one at a time. Each was left to cure for 24 hours before the next was applied.

The first stage of assembly required aligning the ribs along the spar and fixing them in place with fiberglass reinforced epoxy (Figure 7-7). An aluminum tube was selected as an additional stiffing element for the trailing edge of the wing and fixed in place using fiberglass reinforced epoxy (Figure 7-8).

Figure 7-7 Rib Alignment

Figure 7-8 Trailing Edge Stiffening Element

The final task of the wing assembly was to join the leading edge shell with the skeleton. The female mold was used for aligning the two, and tensioned lines were added to ensure proper contact. Fiberglass reinforced epoxy was applied to all contact points (Figure 7-9).

Figure 7-9 Skeleton & Shell curing

After two day of curing, the final assembly was removed from the mold, and wrapped in an ultraviolet light resistant thermoplastic (Figure 7-10). The material shrinks significantly when heated, adding substantial stiffness to the overall structure.

Figure 7-10 Final wing without outer skin

7.2 MATLAB QUASI STEADY-STATE VELOCITY PREDICTION CODE

Written by Patrick Rynne

```
%WASP 2.0 calculates the quasi steady-state velocity of a 2.4 Meter %Class Sailboat in flat water while not allowing roll angles greater %then 45 degrees. Input: wing area, and mass  of counterweight.
%Optional Input: Wind Direction, Heading
%Output: Apparent Wind Angles, Velocity, Roll Angle, Wing Angle of %Attack

% Lower Level Controller

% 1.) Retrieve Heading from upper level controller
% 2.) Retrieve current heading of boat
% 3.) Retrieve current wind direction
% 4.) Retrieve current wind speed
%       - Calculate Re
%       - Determine Xfoil data set

% 5.) Calculate wing angle of attack for proper balance using Xfoil %data set (CL & CD)

Windspeed=input('What is the wind velocity in knots?');

U=(Windspeed)*(0.5144);


%Below options are optional. The current configuration analyzes all %apparent wind angles.
%Winddirection=input('What direction is the wind blowing from? (0-360 %degrees)');
%wind=Winddirection;

%Start with wind direction due North
```

```
wind=0;

%Below options are optional. The current configuration analyzes all %apparent wind angles.
%Hulldirection=input('What direction is your boat initially pointing %(0-360 degrees)?');
%hull=Hulldirection;

%Start with heading due North
hull=0

%Define mass of Wing for roll balance
WW=input('What is the weight of the wing (Kg)? (type "0" for default weight prediction of 20kg)');
if WW==0
WW=20;
end

%Define mass of counterweight in keel
WK=input('What is the weight of the keel ballast(Kg)? (type "0" for default weight prediction of 250kg)');
if WK==0
   WK=250;
end

%Define one-sided surface area of wing. Assume wingspan is 4.5 meters
A=input('What is the one sided wing surface area? (type "0" for default area prediction of 4.5m^2)');
if A==0
   A=4.5;
end

%Condition for ending the analysis once the apparent wind angle = 180 degrees
while hull<181

%Law of Compass - Determines proper value of apparent wind angle based on compass headings
if hull>=wind
   if (hull-180)<wind
   beta=hull-wind
   elseif (hull-180)>wind
   beta=hull-360-wind
else end
else end

if wind>hull
   if (wind-180)<hull
   beta=wind-hull
   elseif wind-180>hull
   beta=hull+360-wind
else end
else end

if beta==0
display 'The WASP is Head to Wind'
else end

if abs(beta)==180
display 'The Wasp is Running with the Wind'
else end
```

```
if beta>0
   if beta>180
   display 'The WASP is on Starboard Tack'
   elseif beta<180
   display 'The WASP is on Port Tack'
   else end
else end

if beta<0
   if beta>-180
   display 'The WASP is on Starboard Tack'
   elseif beta<-180
   display 'The Wasp is on Port Tack'
   else end
else end;

%Density of air (SI units) @ 20 degrees celsius
row=1.2;

%Initial wing angle of attack (maximum power)
alfa=10

%Define CL & CD in terms of angle of attack "alfa" from xfoil modeling %of relationship between Cl &
CD and Alfa over a wind range of 5-30 %knots
if abs(beta)>135
   CL=0;
   CD=1.2;
elseif abs(beta)<=135
   CL=(-.0002*(alfa^3))+(0.0018*(alfa^2))+(0.114*alfa);
   CD=(-.00002*(alfa^3))+(0.0009*(alfa^2))+(0.0015*alfa)+0.00991;
else end

%Theta is function of CL & CD, a function of windspeed
theta=atand(CD/CL);

% Calculate side force and driving force
FAR=sind(abs(beta)-theta)*sqrt((0.25*(row^2)*(U^4)*(A^2))*((CL^2)+(CD^2)));
FAS=cosd(abs(beta)-theta)*sqrt((0.25*(row^2)*(U^4)*(A^2))*((CL^2)+(CD^2)));

%Roll Criteria, moment balance to ensure upright stability
%Determine equlibrium roll angle and make sure it is less
%than 45 degrees. If it is not, angle of attack is reduced.
while ((2.83*(abs(FAS)+sind(45)*WW)))>(sind(45)*WK)
   display 'The WASP is overpowered'
   alfa=alfa-1
   if abs(beta)>135
   CL=0;
   CD=1.2;
 elseif abs(beta)<=135
   CL=(-.0002*(alfa^3))+(0.0018*(alfa^2))+(0.114*alfa);
   CD=(-.00002*(alfa^3))+(0.0009*(alfa^2))+(0.0015*alfa)+0.00991;
else end
   FAS=cosd(abs(beta)-theta)*sqrt((0.25*(row^2)*(U^4)*(A^2))*((CL^2)+(CD^2)));
   FAR=sind(abs(beta)-theta)*sqrt((0.25*(row^2)*(U^4)*(A^2))*((CL^2)+(CD^2)));
   if alfa==0, break, end
```

```
end

%Downwind criteria, turn wing to 90 degrees for maximum driving force
%If apparent wind angle is greater then 135
if abs(beta)>135
   alfa=90;
end

%Determine equilibrium heel angle
HEELANGLE=asind((2.83*FAS)/(WK-2.83*WW))

%Redefine Terms
DrivingForce=FAR
SideForce=FAS
XForce=FAR.*sind(hull)+FAS.*sind(hull+90);
YForce=FAR.*cosd(hull)+FAS.*cosd(hull+90);
LeewayAngle=atand(FAS/FAR);

%Wetted Surface Area
WSA=3.3;

%Density Sea Water
roww=1025;

%Waterline length with 0.7 correction for Larson analysis
L=0.7*3.35;

%Sea Water Viscosity
v=0.00000183;

%Create subgroups for simplicity (ignore)
c1=0.5*roww*WSA;
c2=L/v;

%Define Boatspeed Range in Knots
boatspeed=linspace(0.1,5,100);

%Convert to SI units
x=(boatspeed*0.514);

%Calculate Reynolds Number
re=(x.*L)./(v);

%Calculate Frictional Coefficient from 1957 ITTC Flat Plate
cf=(0.075)./((log10(re)-2).^2);

%Calculate total drag through YD-40 Delft Series Approximation
Drag=(c1.*(x.^2).*cf)*(2.941);

%Find when drag equals driving force
n=1;
while FAR-Drag(n)>0
   n=n+1;
end
```

```
%Find Maximum Speed
maximumvelocity=boatspeed(n)

figure(1); plot(beta,maximumvelocity,'--rs');hold on;
figure(2); plot(beta,HEELANGLE,'--rs');hold on;
figure(3); plot(beta,alfa,'--rs');hold on;

hull=hull+3
end

figure(1);xlabel('Apparent Wind Angle (Degrees)','fontsize',12,'fontweight','b');ylabel('Maximum Velocity
(Knots)','fontsize',12,'fontweight','b');title('Velocity Prediction','fontsize',12,'fontweight','b');
figure(2);xlabel('Apparent Wind Angle (Degrees)','fontsize',12,'fontweight','b');ylabel('Equilibrium Roll
Angle (Degrees)','fontsize',12,'fontweight','b');title('Roll Prediction','fontsize',12,'fontweight','b');
figure(3);xlabel('Apparent Wind Angle (Degrees)','fontsize',12,'fontweight','b');ylabel('Wing Angle of
Attack (Degrees)','fontsize',12,'fontweight','b');title('Angle of Attack
Prediction','fontsize',12,'fontweight','b');
hold off;hold off;hold off;
```

7.3 WASP CONTROL CODE

Written by Michael Tall & Christopher Williams

```
/*
 *  WASP.h.
 *
 */

#include <Carbon/Carbon.h>
#include <stdio.h>
#include <targets/LPC2000.h>
#include <targets/liblpc2000.h>
#include <ctl_api.h>
#include <math.h>
#include "mike_defines_it.h"
#define PI 3.1416
#define SQR(x) x*x

double total_length;
static unsigned char rxchar;
static int timer1Count;
float speed;
unsigned long tmrcap,curr;
unsigned long deltat;
unsigned long prtmrcap = 0;
static unsigned char gpschar;
char GPSMessage[95];
char CompassMessage[50];
int winddirection;
int new_vane,old_vane,last_vane;
double psidesired;
float oldwind = 0;
```

```
unsigned long timer_counter = 0;
unsigned int HAVE_WIND_DIR = 0;
int turn_left, turn_right;
float dwdt;
int sailsteps;
unsigned int High_Sys_Freq = 16; //Hertz
float ratio = 0.0625;
unsigned short consistent_vane_counter = 0;
double latdegF,latminF,londegF,lonminF;
double FinalLat,FinalLong;
static unsigned char gpschar;
double hdng,ptch,rll,tmp,utc,spovgr,covgr,date;
unsigned short GPS_DATA;


/*Function Declarations*/
void GPSInitialize(void);                                   //Setup initial configuration of GPS
void GetGPSMessage(void);

unsigned char ParseGPSMessage(unsigned char MessageType);
unsigned char ParseCompassMessage(unsigned char MessageType);
void delay(int n);
void UART0WriteChar(unsigned char ch);
void UART1WriteChar(unsigned char ch);
unsigned char UART0ReadChar(void);
unsigned char UART1ReadChar(void);
int UART0ReadAvailable(void);
int UART1ReadAvailable(void);
void UART0Initialize(unsigned int baud);
void UART1Initialize(unsigned int baud);
void __putchar(int ch);
void GetGPSMessage(void);
void setGPSGPIO(void);
void setDataloggerGPIO(void);
void setcontrolsailGPIO(void);
void setRuddercontrolGPIO(void);

void GPSInitialize(void);

int read_AD0_1(void);
static void timer0CAP3ISR(void);

float calcwindspeed(void);
void PWMinit(double total_length);
void set_duty(double duty_cycle, double total_length);
void setrudder(void);
void setsail(void);
int get_vane_dir(void);

void logthedata(void);
static void timer1ISR(void);

int attack_angle(int wind_angle);
void adjust_sail(void);
```

```
/**********************************MAIN PROGRAM*****************************/

int main(void)
{

  unsigned long pclk;
  unsigned int frequency = 20000;      //20kHz, to run motor.
  double duty_cycle = 5;
  int mag = 0;
  int vane_data[5000];

  PINSEL0 &= 0;
  PINSEL1 &= 0;
  /*************setup PMW for Motor**********************/

  //clcfrq = OSCILLATOR_CLOCK_FREQUENCY;
  pclk = liblpc2000_get_pclk(liblpc2000_get_cclk(OSCILLATOR_CLOCK_FREQUENCY));
  //total_length  = (pclk / frequency);
  //pbcclk = liblpc2000_get_cclk(OSCILLATOR_CLOCK_FREQUENCY);
  //PWMinit(total_length);

  /****************Initialize UART's********************/
  UART0Initialize(38400);

  /****************Setup Interupts**********************/


  T0PR = 0; //prescale register = 0
  T0CTCR = 0x00;//sets timer mode
  T0TCR = 0x03;//clear and enable the timer count
  T0TCR = 0x01;//enable and initialize the timer count
  T0CCR = 0x0A00;//capture on CAP0.3 on rising edge; a seq. of 0 then 1 causes T0CR3 to be load with
the contents of TC

  T1TCR = 0; /* Reset timer 0 */
  T1PR = 0; /* Set the timer 0 prescale counter */
  T1MR0 = (pclk/High_Sys_Freq)- 1; /* Set time 1 match register to generate an interrupt at 1Hz */
  T1MCR = 3; /* Generate interrupt and reset counter on match */
  T1TCR = 1; /* Start timer 0 */

  ctl_set_isr(5, 0, CTL_ISR_TRIGGER_FIXED, timer1ISR, 0);
  ctl_unmask_isr(5);

  ctl_set_isr(4, 1, CTL_ISR_TRIGGER_POSITIVE_EDGE, timer0CAP3ISR, 0);
  ctl_unmask_isr(4);

  ctl_global_interrupts_enable();


  AD0CR = 0x00210002; // setup A/D AD0.1 input (pin 13) and AD0.2 input (pin 14), 11 clocks/10 bits

  PINSEL1 = 0x09000000;


  old_vane = get_vane_dir();
```

```
 sailsteps = attack_angle(old_vane) * 14.75;
 adjust_sail();
 last_vane = old_vane;


 mag = 0;
 timer_counter = 0;
 GPS_DATA = FALSE;

 while(timer_counter < 230400)
 {

  if (timer_counter % 48 == 0)
  {
   GPS_DATA = TRUE;
   setGPSGPIO();
   GetGPSMessage();
   delay(5000);
   setDataloggerGPIO();
   printf(GPSMessage);
   delay(5000);
   printf(",%d,%0.2f,%d\r\n",get_vane_dir(),calcwindspeed(),(int)(timer_counter / 16));
   delay(5000);
   GPS_DATA = FALSE;
  }
 }


 return 1;

}

int attack_angle(int wind_angle)
{
  if ((wind_angle >= 180) && (wind_angle < 315))
    wind_angle = wind_angle - 15;
  else if ((wind_angle >= 45) && (wind_angle < 180))
    wind_angle = wind_angle + 15;
  else if (wind_angle >= 315)
    wind_angle = wind_angle - 90;
  else
    wind_angle = wind_angle + 90;

  if (wind_angle > 360)
    wind_angle = wind_angle - 360;
  if (wind_angle < 0)
    wind_angle = wind_angle + 360;

  return wind_angle;
}


int get_vane_dir(void)
{
```

```
 unsigned short read_ad;
 float winddir;

 AD0CR = 0x00210002; // setup A/D AD0.1 input (P0.28, pin 13), 11
 //clocks/10 bits
 AD0CR |= 0x01000000; // start conversion
 while (AD0GDR == 0x8000000); // wait for DONE to go high
 read_ad = AD0DR1; // get ADC data
 read_ad = ((read_ad >> 6) & 0x03FF); // extract result

 winddir = read_ad * 360 / 1023;

 return winddir;
}


void adjust_sail()
{
   setcontrolsailGPIO();
   printf("@0P-%d\r", sailsteps);
   delay(5000);
   printf("@0G\r");
   delay(50000);
}


static void timer1ISR(void)
{
 float temp;

 timer_counter++;

 if (!GPS_DATA)
 {
   new_vane = get_vane_dir();

   if (last_vane == new_vane)
     consistent_vane_counter++;
   else
     consistent_vane_counter = 0;

   last_vane = new_vane;

   if (consistent_vane_counter == 10)
   {
     consistent_vane_counter = 0;
     HAVE_WIND_DIR = TRUE;
     old_vane = new_vane;
     sailsteps = attack_angle(new_vane) * 14.75;
   }
   else
   {
     //Check for falsies
     turn_left = old_vane - new_vane;
     turn_right = new_vane - old_vane;
```

```
      if (turn_left < 0)
        turn_left += 360;
      if (turn_right < 0)
        turn_right += 360;

      if (turn_left > turn_right)
      {
        temp = turn_right / ratio;
        if (temp > 155)
        {
          HAVE_WIND_DIR = TRUE;
          old_vane = new_vane;
          sailsteps = attack_angle(new_vane) * 14.75;
        }
      }
      if (turn_right > turn_left)
      {
        temp = turn_left / ratio;
        if (temp > 155)
        {
          HAVE_WIND_DIR = TRUE;
          old_vane = new_vane;
          sailsteps = attack_angle(new_vane) * 14.75;
        }
      }
    }

    if (HAVE_WIND_DIR)
    {
      HAVE_WIND_DIR = FALSE;
      adjust_sail();
    }
  }


  T1IR = 0xFF;
}




void delay(int n)
{
  volatile int i;
  for (i = 0; i < n; ++i);
}

void UART0WriteChar(unsigned char ch)
{
  while ((U0LSR & 0x20) == 0);
  U0THR = ch;
}

void UART1WriteChar(unsigned char ch)
```

```
{
 while ((U1LSR & 0x20) == 0);
 U1THR = ch;
}

unsigned char UART0ReadChar(void)
{
 while ((U0LSR & 0x01) == 0);
 return U0RBR;
}

unsigned char UART1ReadChar(void)
{
 if ((U1LSR & 0x01) == 0);
 return U1RBR;
}

int UART0ReadAvailable(void)
{
 return U0LSR & 0x01;
}

int UART1ReadAvailable(void)
{
 return U1LSR & 0x01;
}

void UART0Initialize(unsigned int baud)
{
 /* Configure UART */
 unsigned int divisor =
liblpc2000_get_pclk(liblpc2000_get_cclk(OSCILLATOR_CLOCK_FREQUENCY)) / (16 * baud);
 U0LCR = 0x83; /* 8 bit, 1 stop bit, no parity, enable DLAB */
 U0DLL = divisor & 0xFF;
 U0DLM = (divisor >> 8) & 0xFF;
 U0LCR &= ~0x80; /* Disable DLAB */
 PINSEL0 = 0x00058005;
 //PINSEL1 = 0x09000000;
 U0FCR = 1;
}
void UART1Initialize(unsigned int baud)
{
 /* Configure UART */
 unsigned int divisor =
liblpc2000_get_pclk(liblpc2000_get_cclk(OSCILLATOR_CLOCK_FREQUENCY)) / (16 * baud);
 U1LCR = 0x83; /* 8 bit, 1 stop bit, no parity, enable DLAB */
 U1DLL = divisor & 0xFF;
 U1DLM = (divisor >> 8) & 0xFF;
 U1LCR &= ~0x80; /* Disable DLAB */
 U1FCR = 1;
}

void __putchar(int ch)
{
 if (ch == '\n')
```

```
   UART0WriteChar('\r');
  UART0WriteChar(ch);
}


void GetGPSMessage(void)
{
  char tempchar;
  int index;

  do {
     tempchar=UART0ReadChar();
    } while(tempchar !='$');
  index=0;
  do {
       tempchar=UART0ReadChar();
       GPSMessage[index]=tempchar;
       index=index+1;
     } while ((tempchar!='*')&&(index<95));
  GPSMessage[index]=0;
}


/*******************Set Multiplexer to GPIO.x************************/
void setGPSGPIO(void)
{
  IO0DIR = 0x003E0000;
  IO0SET = 0x003C0000;
  IO0CLR = 0x00020000;
  delay(500);
}

void setDataloggerGPIO(void)
{
  IO0DIR = 0x003E0000;
  IO0SET = 0x00360000;
  IO0CLR = 0x00080000;
  delay(500);
}

void setcontrolsailGPIO(void)
{
  IO0DIR = 0x003E0000;
  IO0SET = 0x002E0000;
  IO0CLR = 0x00100000;
  delay(500);
}

void setRuddercontrolGPIO(void)
{
  IO0DIR = 0x003E0000;
  IO0SET = 0x001E0000;
  IO0CLR = 0x00200000;
  delay(500);
}
```

```
void setCompassGPIO(void)
{
 IO0DIR = 0x003E0000;
 IO0SET = 0x003A0000;
 IO0CLR = 0x00040000;
 delay(500);
}

void GPSInitialize(void)
{
        puts("$PMTK313,1*2E\r\n");  //enable SBAS (WAAS) satellite
        delay(100); //100mS delay
        puts("$PMTK301,2*2E\r\n");//set DGPS source to WAAS
        delay(100); //100mS delay
        puts("$PMTK314,0,5,0,0,0,0,0,0,0,0,0,0,0,0,0,0,0,0,0*2D\r\n");   //only enable RMC output sentence
every fix
        delay(100); //100mS delay
}



/*timer interupt to find windspeed using CAP0.3*/
static void timer0CAP3ISR(void)
{
   tmrcap = T0CR3;      // read the capture value
   deltat = tmrcap - prtmrcap;
   prtmrcap = tmrcap;
   VICVectAddr  = 0x00000000;              //Dummy write to signal end of interrupt
   T0IR = 0x80;                    //Clear cap0.3 interrupt
}

float calcwindspeed(void)
{
 speed = ((14745600.0/((double)deltat))*2)*1.25;
 return speed;
}

void PWMinit(double total_length)
{
 PINSEL0 |= 0x00008000;    //Enable pin 0.7    as PWM2

 PWMPR = 0x00000000;       //Load prescaler
 PWMPCR = 0x00000400;      //PWM channel 2, pin 7 single edge control, output enabled
 PWMMCR = 0x00000003;      //On match with timer reset the counter
 PWMMR0 = total_length;    //set cycle rate
 PWMMR2 = 0;             //set falling edge of PWM2
 PWMLER = 0x00000007;      //enable shadow latch for match 0 - 2
 PWMTCR = 0x00000002;      //Reset counter and prescaler
 PWMTCR = 0x00000009;      //enable counter and PWM, release counter from reset
}

void set_duty(double duty_cycle, double total_length)
{
```

```
 PWMMR2 = total_length*(duty_cycle / 100);
 PWMTCR = 0x00000009;
}

void setrudder(void)
{
 setRuddercontrolGPIO();// this enables the multiplexer pin set for the ruddercontrol

 delay(1000);
 printf("@0A500\r");
 delay(1000);
 printf("@0B300\r");
 delay(1000);
 printf("@0M400\r");
 delay(1000);
 printf("@0T1\r");
 delay(1000);
 printf("@0Z0\r");
}

void setsail(void)
{
 setcontrolsailGPIO();// this enables the multiplexer pin set for the controlsail

 delay(1000);
 printf("@0A500\r");
 delay(1000);
 printf("@0B300\r");
 delay(1000);
 printf("@0M400\r");
 delay(1000);
 printf("@0T1\r");
 delay(1000);
 printf("@0Z0\r");
}


void logthedata(void)
{
   /*setDataloggerGPIO();
   delay(1000);
   printf("\n");
   printf("%f \n",utc);
   puts(fixstatus);
   puts(latitude);
   puts(latsec);
   puts(longitude);
   puts(longsec);
   printf("%f \n",spovgr);
   printf("%f \n",covgr);
   printf("%f \n",date);
   puts(navmode);
   printf("\n\n");
   printf("%f \n",hdng);
   printf("%f \n",ptch);
```

```
    printf("%f \n",rll);
    printf("%f \n",tmp);
    printf("\n\n");
    printf("%f\n\n", winddirection);
    printf("%f\n\n", speed);
    printf("\n\n");*/
}



/* mike_defines_it.h
*/

#define FALSE 0
#define TRUE 1
#define IDLE 0
#define GP 1
#define COMPASS 2
#define DATALOGGER 3
#define OBJECT_DETECTION 4

#define pin2 0x00000004
#define pin5 0x00000020
#define green_led 0x00002000
#define pin_017 0x00020000
#define pin_018 0x00040000
#define pin_019 0x00080000
#define pin_020 0x00100000

//GPS defines to be used with printf \r = carriage return \n = new line
//Used with the SIRF3 Chipset (GlobalSat EM408)
#define OFF_GGA "$PSRF103,00,00,00,01*24\r\n"
#define OFF_GLL "$PSRF103,01,00,00,01*25\r\n"
#define OFF_GSA "$PSRF103,02,00,00,01*26\r\n"
#define OFF_GSV "$PSRF103,03,00,00,01*27\r\n"
#define OFF_RMC "$PSRF103,04,00,00,01*20\r\n"
#define OFF_VTG "$PSRF103,05,00,00,01*21\r\n"
#define QUERY_GGA "$PSRF103,00,01,00,01*25\r\n"
#define QUERY_GLL "$PSRF103,01,01,00,01*24\r\n"
#define QUERY_GSA "$PSRF103,02,01,00,01*27\r\n"
#define QUERY_GSV "$PSRF103,03,01,00,01*26\r\n"
#define QUERY_RMC "$PSRF103,04,01,00,01*21\r\n"
#define QUERY_VTG "$PSRF103,05,01,00,01*20\r\n"
#define NEMA_9600 "$PSRF100,1,9600,8,1,0*0D\r\n"
#define NEMA_38400 "$PSRF100,1,38400,8,1,0*3D\r\n"

//PINSEL0 defines
//Clear PINSEL0 out
//To use values below -> PINSEL0 |= whatever #define is wanted
//Also used as TxD UART0
#define PWM1 0x00000002
#define PWM2 0x00008000
//Also used as RxD UART0
#define PWM3 0x00000008
//Also used as TxD UART1
```

```
#define PWM4 0x00020000
//PWM5 is in the PINSEL1 defines
//Also used as RxD UART1
#define PWM6 0x00080000
//TxD UART0 transmit data
//Also used as PWM1
#define TxD_0 0x00000001
//RxD UART0 recive data
//Also used as PWM3
#define RxD_0 0x00000004
//TxD UART1 transmit data
//Also used as PWM4
#define TxD_1 0x00010000
//RxD UART1 recive data
//Also used as PWM6
#define RxD_1 0x00040000

//PINSEL1 defines
//Clear PINSEL0 out
//To use values below -> PINSEL1 |= whatever #define is wanted
#define PWM5 0x00000400

//PWMPCR
#define PWM4_SINGLEEDGE_OUTPUTE 0x00001000
#define PWM2_SINGLEEDGE_OUTPUTE 0x00000400
#define PWM5_SINGLEEDGE_OUTPUTE 0x00002000

//PWMMCR
#define PWMMR0_INTERRUPT_RESET 0x00000003

//GPIO
#define GPIO_P017_OUTPUT 0x00020000
#define GPIO_P018_OUTPUT 0x00040000
#define GPIO_P019_OUTPUT 0x00080000
#define GPIO_P020_OUTPUT 0x00100000
#define GPIO_P004_OUTPUT 0x00000010
```

8 References

[1] U.S. Commission on Ocean Policy, "U.S. Ocean Action Plan", 2004, 4-5.

[2] The National Office for Integrated and Sustained Ocean Observations, "IOOS Development Plans" *in U.S. Ocean Report No. 9*, Silver Spring MD, 2007.

[3] D. Paley, N. Leonard, "Mobile Sensor Networks for Oceanographic Sampling", *Princeton University Graduate Research Symposium* (2004)

[4] E.W Schlieben, "SKAMP – An Amazing Unmanned Sailboat!", *Ocean Industry*, (1969) 38-43.

[5] G. H. Elkaim, "The Atlantis Project: A GPS Guided Wing-Sailed Autonomous Catamaran" Ph.D diss., Stanford University, 2002.

[6]G.H. Elkaim, C.O. Boyce, "Energy Scavenging and Aerodynamic Performance of a Rigid Wing Propulsion System for an Autonomous Surface Vessel", *In Proceedings ION Global Navigation Satellite Systems Conference*, 2008.

[7] "*The Microtransat Challenge"*, www.microtransat.org, 2008

[8]Sauze, C., M. Neal. "Design Considerations for Sailing Robots Performing Long Term Autonomous Oceanography", *In Proceedings of the 2008 International Robotic Sailing Conference*, 2008.

[9] Covarrubias Photography, "Stars & Stripes", San Diego, CA. 1988

[10] Team Invictus, "Little America's Cup", Bristol RI. 2004

[11] Gilles Martin - Raget, "BMW Oracle Extreme 40 Capsize", Valencia ESP, 2008

[12] Anna Tunnicliffe, Plantation FL, 2008

[13] Team Alinghi, "32nd Defense of the Americas Cup", Valencia ESP, 2006

[14] International 2.4 Metre Class Association, "Class Specifications Diagram", 2007

[15] L. Larson, R. Eliasson, *Principles of Yacht Design*, Blacklick, Ohio: The McGraw-Hill Companies, 2000.

[16] J.D Anderson, *Fundamentals of Aerodynamics*, Blacklick, Ohio: The McGraw-Hill Companies, 1984.

[17] M. Drela, "XFOIL and Low Speed Airfoil Design" in *Proceedings of Engineering Design and Rapid Prototyping Course*, Massachusetts Institute of Technology, Cambridge Massachusetts 2005.

[18]M. M Koochesfahani, V. Smiljanovski, "Initial Acceleration Effects on Flow Evolution Around Airfoils Pitching to High Angles of Attack", *AIAA Journal*, Volume 31, NO. 8. (1993)

[19] F. Bethwaite, *High Performance Sailing*, Camden Maine: International Marine, 1993.

[20] J.A. Keuning, U.B. Sonnenberg, "Approximation of the Hydrodynamic Forces on a Sailing Yacht based on the Delft Systematic Yacht Hull Series", in *Proceedings of The International HISWA Symposium on Yacht Design and Yacht Construction*, 1998.

[21] C. Baker *et al*. "A Wind & Solar-Powered Autonomous Surface Vehicle", Senior Design Final Report, Florida Atlantic University, 2008.

[22] Google Maps, Google Inc. 2008.

[23] The American Meteorological Society, "A Maury Project Module: Density-Driven Ocean Circulation", in *Proceedings of The International Conference on School and Popular Meteorological and Oceanographic Education,* 2002.

[24] Honeywell Inc, "Oxidation Reduction Potential Measurement for Microbiological Control in Makeup Water and Cooling Water", Honeywell Sensor Systems Applications, Golden Valley Minnesota, 2008.

[25] M.R Benjamin *et al*. "Navigation of Unmanned Marine Vehicles in Accordance with the Rules of the Road", in *Proceedings of the 2006 IEEE International Conference on Robotics and Automation*, 2006.

[26] J.R. Higinbotham, J.R. Moisan. "Development of a New Long Duration Solar Autonomous Surface Vehicle", in: *Proceedings of the 2006 MTS/IEEE OCEANS Conference.* 2006.

[27] S. Showalter, “Are All Floating Structures Vessels? An Analysis of the U.S. Supreme Court’s Holding in Stewart v. Dutra Construction Company”, in: *Proceedings of the 2006 MTS/IEEE OCEANS Conference*. 2006.